Review

Possible Physical Basis of Mirror Symmetry Effect in Racemic Mixtures of Enantiomers: From Wallach's Rule, Nonlinear Effects, B–Z DNA Transition, and Similar Phenomena to Mirror Symmetry Effects of Chiral Objects

Valerii A. Pavlov [1],*, Yaroslav V. Shushenachev [2] and Sergey G. Zlotin [1]

[1] N. D. Zelinsky Institute of Organic Chemistry, Russian Academy of Sciences, 119991 Moscow, Russia; zlotin@ioc.ac.ru

[2] OOO 'Avrora Service' Ltd., 119991 Moscow, Russia; slavash@mail.com

* Correspondence: pvlv69@mail.ru; Tel.: +07-495-750-2545

Abstract: Effects associated with mirror symmetry may be underlying for a number of phenomena in chemistry and physics. Increase in the density and melting point of the 50%L/50%D collection of enantiomers of a different sign (Wallach's rule) is probably based on a physical effect of the mirror image. The catalytic activity of metal complexes with racemic ligands differs from the corresponding complexes with enantiomers as well (nonlinear effect). A similar difference in the physical properties of enantiomers and racemate underlies L/D inversion points of linear helical macromolecules, helical nanocrystals of magnetite and boron nitride etc., B–Z DNA transition and phenomenon of mirror neurons may have a similar nature. Here we propose an explanation of the Wallach effect along with some similar chemical, physical, and biological phenomena related to mirror image.

Keywords: racemate and mirror effect; C_1- and C_2-symmetric catalysis; Z-DNA defect; mirror neurons; baryonic asymmetry

1. Introduction

Studies on related phenomena carried out in parallel in different fields of science may appear fruitful. From this viewpoint, it would be interesting to analyze physical essentials of a chemical phenomenon such as Wallach's rule (an increase in the density and change in the other properties of the 50%/50% mixture of L and D enantiomers in comparison with enantiomers in crystal and in solution). Asymmetric catalysis using non-enantiopure chiral ligands occurs sometimes with a deviation from the linear relation between optical purity of the product and ligand (nonlinear effects). The mechanism of this phenomenon should be based on a difference between the catalytic activity of complexes with homochiral and heterochiral (racemic) ligands. Is there an internal connection between Wallach's rule and nonlinear effects?

The research and analysis of *P/M* points of helicity inversion of polymers and macrostructures formed from achiral molecules is also of great interest. Such helicity inversion points, as present in both the linear and surface arranged (domains) structures of macromolecules, are apparently their common feature, which is likely to have a common basis with Wallach's rule. Chirality inversion points were also found in linear inorganic structures (boron nitride, hematite in magnetic field, etc.). Similar inversion points are observed even in a very strong and highly organized "reinforced" double helix, e.g., DNA (B–Z DNA transition).

A change in properties similar to that by Wallach's rule is possible even for water currents. It could underpin a hypothetical explanation of the mysterious and unexplained accident at the Sayano-Shushenskaya Hydro Power Plant on 17 August 2009. Assumingly, a spontaneous high-pressure water current in the form of two intertwining fluxes of the opposite chirality sign (like braided hair) could cause the accident. Such a structure, according to Wallach's rule for the 50%/50% mixture of molecules with mirror symmetry, could increase the density of the water flux supplying the turbine.

The external physical factor of the symmetry influence may also explain the origin of biological homochirality. This assumption relies on a direct parallel in symmetry of right-handed helical structures of the main macromolecular triad (polypeptides, DNA, and polyglucanes) and the right-handed helical trajectory of the Moon, Earth, Sun, and Milky Way.

The search for common features and patterns of all these phenomena has not been previously carried out. This review is an attempt to find such similarities in some chemical, physical and biological related effects (phenomena).

2. Wallach's Rule

Back in 1895, Wallach [1] found that a pair of enantiomers sometimes co-crystallize, giving crystals of true racemates higher melting points than their chiral counterparts (Figure 1a). Brock et al. [2] coined the term "Wallach's rule" for the empirical finding that racemic crystals tend to have a higher density than their pure enantiomeric counterparts. It is currently believed that a collection of right- and left-handed enantiomers can have tighter packing (more than 4–6% denser) than a collection of pure enantiomers [3–28]. Solubility experiments show that racemates tend to be slightly more stable than their chiral counterparts [6,29,30]. Thus, the difference between enantiomers and true racemates is preserved in solution as well.
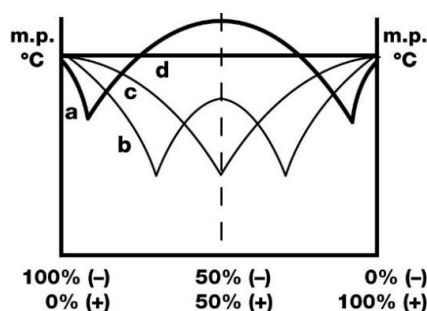

Figure 1. Basic types of the relationship between the melting point of enantiomer mixtures and the composition: (**a**)—true (Wallach) racemates, (**b**)—the racemate forms a compound, (**c**)—the racemate is a physical mixture (conglomerate), (**d**)—the racemate forms a solid solution, enantiomers are isomorphous.

However, it is not entirely true that there is a relation between crystal energy (lattice energy) and the crystal density of racemates and enantiomers. Nevertheless, some researchers believe that true racemates are energetically preferable [31], stable [6,29,30] or exist in a more ordered structural form [32] than pure enantiomers. It should be noted that Wallach's rule is probably applicable to more phenomena than it was supposed. For example, the curve (**b**) (Figure 1) can, under elevated pressure, obey Wallach's rule (Figure 2) [33].

For more than a century, a reason for the difference in the crystal form of true racemates and corresponding enantiomers has not been universally accepted. X-ray images of small chiral molecules show that only homochiral dimers were detected in the unit cell of the racemate [12]. It is believed that left- and right-handed enantiomers have an additional capability of a "favorable packing arrangement" [2]. However, it is a statement of fact rather than an explanation. The simplest explanation of Wallach's rule is the difference in bond energy, e.g., of hydrogen bonds. Such explanation has many supporters [5,7,11,26–28]. However, it is also more like a statement of fact. Besides, many

researchers are convinced that hydrogen bonds are not fundamentally different [8–10,21–28]. Therefore, the reason for Wallach's phenomenon is not clear so far.
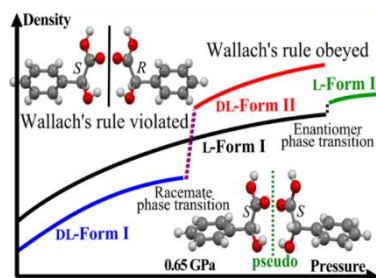

Figure 2. Wallach's rule enforced by pressure in mandelic acid.

An interrelation of enantiomers and the racemate as the subject of Wallach's rule occurs most frequently, but it is not the single case. For example, the (R,S)-crystal of 1,2-dicyclohexylethane-1,2-diol is less dense than (S,S)- or (R,R)-enantiomers, but the melting point of the (R,S)-crystal is almost 10 K higher than that of the enantiomer crystal [18] (Figure 1b). The relationship of crystals of the racemate and enantiomers cannot be evaluated because it is impossible to obtain the racemate crystal even under elevated pressure [34]. The contradictions in Wallach's rule fulfilment were marked by Khrustalev [17], Willer [15] and Podsiadlo [16].

Conformity to Wallach's rule in terms of density was quantified by Kennedy et al. [19] "While average densities conform to Wallach's rule, 6 of the 13 individual pairing do not" [19]. A striking exception to Wallach's rule was reported by Patrik and Brock [18]: crystals of racemic 1,2-dicyclohexyletane-1,2-diol appeared 4% less dense than those of enantiomers.

A special group of crystals forms during crystallization as a mechanical mixture of crystals of two pure enantiomers called a conglomerate (Figure 1c). It is a case of spontaneous resolution [35]. This case is relatively less studied and it less frequently occurs in nature. Pavlov et al. [36] synthesized trans-bis-1*S*,2*S*- and 1*R*,2*R*-(diphenylphosphino)cyclopentanenickel dibromide (Scheme 1).
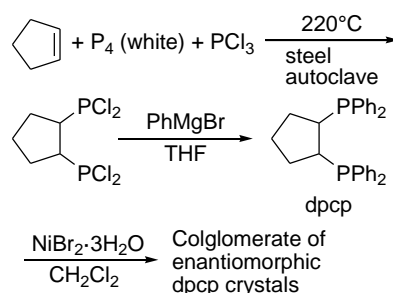
Scheme 1. Synthesis of NiBr$_2$((*R,R*)-dpcp)CH$_2$Cl$_2$ and NiBr$_2$(*S,S*)-dpcp)CH$_2$Cl$_2$ complexes.

The largest prismatic single NiBr$_2$((*R,R*)-dpcp)·CH$_2$Cl$_2$ and NiBr$_2$((*S,S*)-dpcp)·CH$_2$Cl$_2$ crystals were separated manually (Figure 3). A variety of crystals were observed in crystals of different.
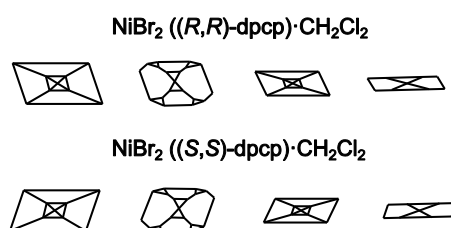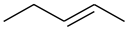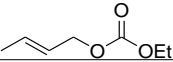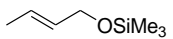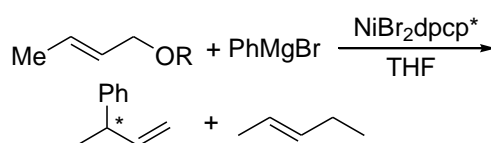

Figure 3. Modifications of the crystals (view along C_2 axis).

Enantiomorphic forms. Diversity was also present in a series of crystals of the same sign of chirality. Assumingly, the obtained well-formed crystals were not enantiomerically pure. This assumption was tested in asymmetric cross-coupling of Grignard reagents with alkenyls (Table 1, Scheme 2) [36].

Table 1. Asymmetric cross-coupling of Grignard reagents (PhMgBr) with alkenyls (R^1Y) on chiral nickel complexes at room temperature.

R^1Y (Y = OR) R^1=	Complex	$CH_3CH(Ph)CHCH_2$ ee% (Conf.)
O (allyl carbonate, O, OEt)	$NiBr_2(R,R)$-dpcp	52(*S*)
	$NiBr_2(S,S)$-dpcp	42(*R*)
OSiMe₃ ($OSiMe_3$)	$NiBr_2(R,R)$-dpcp	67(*S*)
	$NiBr_2(S,S)$-dpcp	58(*R*)

Scheme 2. Asymmetric cross-coupling over $NiBr_2$dpcp chiral complex.

Analogous reactions proceed in the presence of chiral complexes $NiCl_2$-Chiraphos with *ee* = 58% [37], 68% [38] and 89% [38] depending on R^1Y and ArMgBr under similar conditions. However, well-faceted enantiomorphic crystals of $NiBr_2$ (*R,R*)-dpcp and $NiBr_2$(*S,S*)-dpcp complexes as catalysts are not equally high enantioselective in reaction (2) (Table 1) [36]. Therefore, the assumption about the incomplete enantiomeric purity of crystals in the conglomerate remains valid.

Back to Wallach's rule, it should be mentioned that the difference in the melting points of more than 46 °C is very difficult to explain by the intermolecular H-bonding distinctions between the racemate and enantiomers [11]. Additionally, there are a few cases where a true racemate is a crystal and an enantiomer forms a gel [5,37] and vice versa [6]. Additionally, a relationship inverse to Wallach's rule was found [18]. Studies of crystallization thermodynamics [4] and crystal lattice energies [38] indicate that true racemates have lower entropy, higher enthalpy or higher free energy than enantiomers. However, these parameters do not allow an unambiguous understanding of the physical basis of the higher packing density of racemates compared to enantiomers [2]. Therefore, these parameters are rather a result than a reason. Some researchers believe that this structural feature of the racemate-enantiomer phenomenon is "mutually exclusive binding" or "strong enantioselective self-recognition" in true racemates compared to enantiomers [12,39].

A visual representation of the greater density of racemates against enantiomers may be a mutual arrangement of two identical helices of different signs of chirality shown in Figure 4, e.g., denser packing (tight ridges-in-grooves packing) of the left- and right-handed triple helices as compared to the left-handed [40]. It should be noted that even mixing of left- and right-handed helices in solution drastically lowered solubility compared to helices with the same sign of chirality [41,42].

Enantiopure　　Enantiopure　　Racemate

(**a**)　　　　　　　　　　　(**b**)

Figure 4. (**a**) Schematic view of optimal conformations of LD (racemate) (left) and LL (enantiomers) (right) triple helices of collagen, (**b**) N-Stearoil-serine methyl ester in a monolayer under a microscope.

3. Chiral Superstructures from Achiral Molecules, Chiral and Racemic Fields

One may assume that the difference between a racemic mixture and enantiomeric counterpart also has a physical basis. It is possible that, along with a chiral field, there is a racemic field [43]. Indeed, numerous examples confirm the above, e.g., well- known building of a chiral superstructure from achiral molecules. Achiral molecules can be involved in chiral ordering shifting relative to each other around the central axis (π-π staking, hydrogen bonds etc.) along the left or right screw. This synchronization occurs in smectic (lamellar) or nematic liquid crystal (LC) phases. Numerous studies of "banana", "hat" or crown-like nanostructures [44–51] in the LC phase indicate that a ratio of layers with chiral superstructures of different chirality signs is roughly 50%:50%. The layers are observed in photomicrographs between slightly uncrossed polarizers as dark or bright spots (chiral domains). Therefore the phenomenon of "mirror symmetry breaking" [35–42] can only refer to one individual domain or a monolayer with superstructures of the similar chirality sign. Thus, a ratio of chiral domains (bright/dark spots) is close to racemic (50%/50%). Therefore, this crystallization with the racemic macrostructure formation may be stimulated by a physical factor similar to the racemic field [43].

The racemic field is not a universally accepted concept such as the chiral field. A possible reason is that this field manifests itself against the background of a much stronger kinetic factor leading to the racemic product. Therefore, we can assume that the racemic field exists only on the basis of the processes in which the time factor is not determinant. Such process can result in the formation of chiral crystals in natural deposits on Earth. The deposits are known to have been formed over millions of years in the geological conditions of early Earth. All deposits have *l*- and *d*-crystals of quartz [52–56], calcite ($CaCO_3$) [57–59], and gypsum ($CaSO_4 \cdot 2H_2O$) [60,61] are found in approximately equal proportions (50%:50%). Relatively much faster (in laboratory conditions) crystallization of sodium chlorate ($NaClO_3$) from an oversaturated aqueous solution leads to the conglomerate of 50% *l*- and 50% *d*-crystals (Scheme 3) [62]. Crystallization is a sluggish reaction, therefore, the racemic field is likely to play a significant role in it. However, as seen from the Scheme, a random predominance of *l*- or *d*-crystals reaches more than 90% during stirring. In other words,
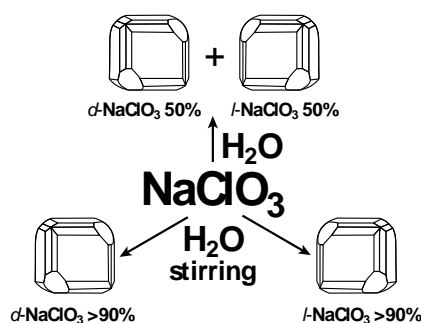
Scheme 3. Influence of reaction mixture stirring (helical flux).

Stirring in a fixed direction results both in *l*- and in *d*-dominated crystallization in different runs. Thus, even rotational energy can be sufficient to break mirror symmetry of the resulting crystallization product. Similar crystallization was also observed for melt 1,1'-binaphthyl (*ee* > 80%) [63,64]. An experiment shown in Figure 5 can give relative evidence of the energy effect of stirring as an inductor of chirality [65].

Stirring with glass beads increases the solution density and accordingly increases the energy effect of stirring. The results are consistent with the idea that even a slight increase in the solution density due to glass beads leads to mirror symmetry breaking. This idea is also confirmed by a decrease in the time passed to achieve maximum enantioselectivity with an increase in the number of glass beads and the stirring rate [65]. The stirring effect on reaction enantioselectivity can be explained by the influence of the chiral field. There are plenty of indications of the chiral field existence in the literature (see, e.g., [43,66,67]). We will cite two examples from the many as evidence of its

existence and connection with stirring or the reaction space structure. The first is that antracene monomers under the action of intensive stirring can self-assemble into a chiral twisted shape during polymerization. The well-defined left-handed helix structure is formed under vigorous stirring during solution evaporation (Figure 6) [68]. The diameter of the helical flow of the reaction solution and the diameter of the polyantracene molecule are incomparable in size (a helix diameters ratio is ~5·10^9/1 nm). Therefore, chirality of the reaction product could only be a result of the helical flux of solution and chiral fields created by the flux.
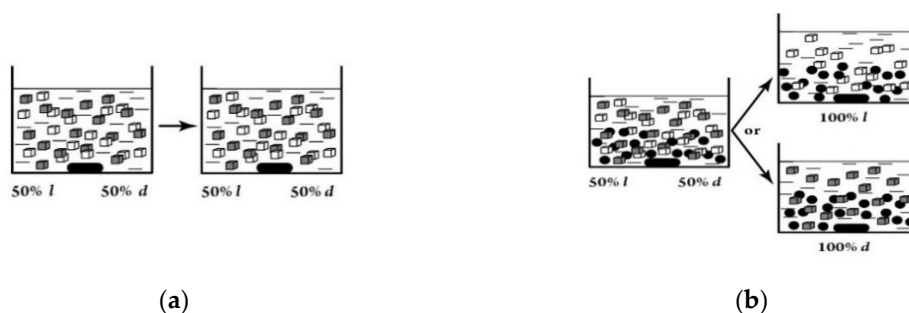

(a)   (b)

Figure 5. Stirring of the mixture of 50% *l*- and 50% *d*-crystals of NaClO$_3$ without glass beads (**a**) and with glass beads (**b**) in the dissolution–crystallization conditions.
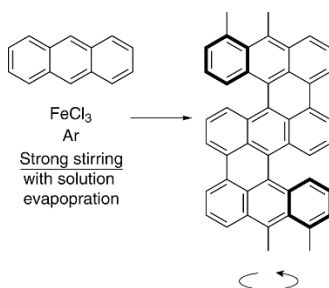

Figure 6. Polyantracene formation with left-handed helical nanoarchitectures.

These experimental data are comparable with the results of stirring during NaClO$_3$ crystallization (Scheme 1). Thus, the hypothesis on the helical flow influence on mirror symmetry breaking has been proven once again. By analogy, chirality occurs due to rotation of the reaction mixture in other reactions. In some cases, as noted, the direction of flows affects the sign of chirality [67–71].

Another example may also illustrate the existence of the chiral field. Hydrogenation of α-acetamidocinnamic acid (ACA) proceeded enantioselectively in the presence of the achiral complex in cholesteric liquid crystal (ChLC) media [72,73]. (Scheme 4) ChLC (cholesteryl tridecanoate), ACA and catalyst molecules in this solution had helical ordering at ChLC mesophase temperature ~65 °C (temperature of maximal chiral ordering). This was evidenced by the fact that the CD spectra of the substrate and catalyst molecules exhibited the induced circular dichroism maxima of the same sign in the absorption bands of these molecules. In these conditions, a temperature–enantioselectivity dependence (ee_{max} = 15%) was observed in the Scheme 4 [72,73]. Meanwhile the ChLC helix pitch (300–400 nm) was much higher than the size of ACA and Wilkinsons catalyst (RhCl(PPh$_3$)$_3$). Hence, it is difficult to explain the chiral information transfer (asymmetric induction) from ChLC to the substrate molecule (ACA) without invoking the chiral field concept. The coincidence of maximum enantioselectivity of the Scheme 4 and maximal chiral ordering ChLC (mesophase temperature ~65 °C) confirms the fact of asymmetric induction from the ChLC chiral helix. The existence of a racemic field may be explained on the basis of the reaction mechanism in the presence of C_2-ligands (Table 2, Scheme 5). A calorimetric study of the reaction kinetics let propose a catalytic cycle (Scheme 6) [74–77]. The racemic field is stabilized by the π-π interaction in the intermediate *C* of the cycle. The existence of the racemic field can explain low enantioselectivity of the reaction (Table 2).
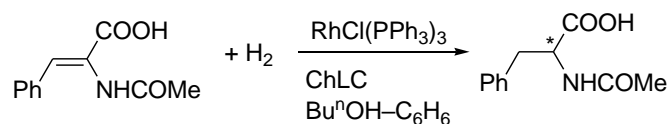
Scheme 4. Hydrogenation of ACA over Wilkinson's catalyst.

Table 2. Results of screening of chiral ligands **1–5**.

L	*ee*%	Config. Product	Ref.
1	8	*S*	[74]
2	8	*R*	[75]
3	26	*S*	[74]
4	20	*R*	[74]
5	4	*S*	[76]

1 R = OH (C_2)
2 R = NMePh (C_2)

3 R = NH$_2$ (C_2)
4 R = OH (C_2)

5 (C_2)
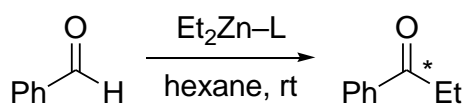
Scheme 5. Diethylzinc addition to bezaldehyde over **1–5** ligands.
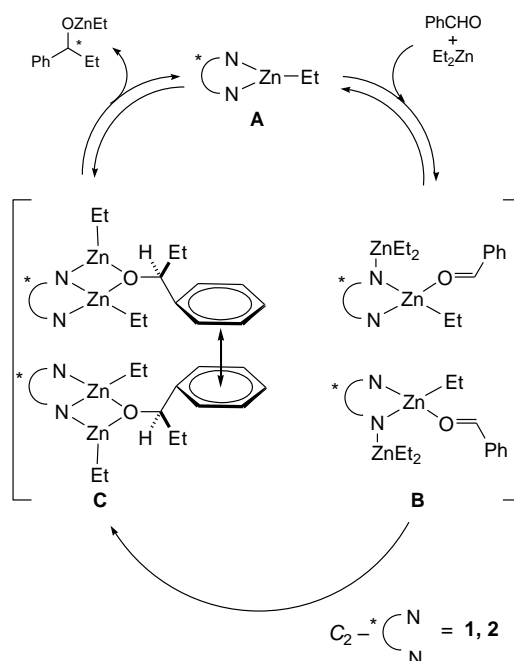
Scheme 6. Possible mechanism of the reaction in Scheme 5 over ligands 1,2.

4. Nonlinear Effects, Asymmetric Induction and Chiral Adsorption

Asymmetric catalysis using non-enantiopure ligands sometimes occurs with a deviation from a linear relationship between optical purity of the product and ligand. The deviation called a 'nonlinear

effect' (NLE) is presented formally in Figure 7 [77]. To understand the mechanism of the NLE occurrence Kagan et al. [78–80]. and Noyori et al. [81–83] proposed two models (Scheme 7) [84]. A few years later, Kitamura, Noyori et al. [85] proposed "simplified" NLE models (Scheme 8). All the schemes explain the NLE appearance by a difference in catalytic and enantioselective properties of monomer-dimeric and homochiral–heterochiral complexes. According to Schemes 7 and 8A,B, heterochiral and homochiral complexes may have different catalytic activity ($k_R \neq k_S$ and $k_{RR} \neq k_{SS}$). Thus, the difference in the catalytic properties of such complexes is on a par with different densities or solubilities of a racemate and enantiomers (Wallach's rule). Additionally, of note is that the temperature influence on the NLE [86,87] is more consistent with the catalytic parameter than with the stereochemical manifestation of this phenomenon.
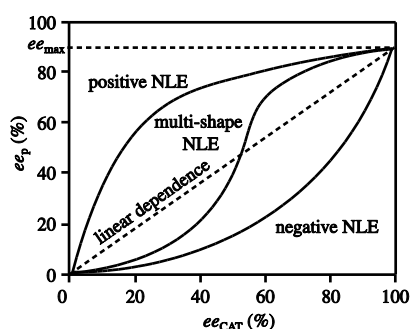
Figure 7. Examples of nonlinear effects in asymmetric catalysis.
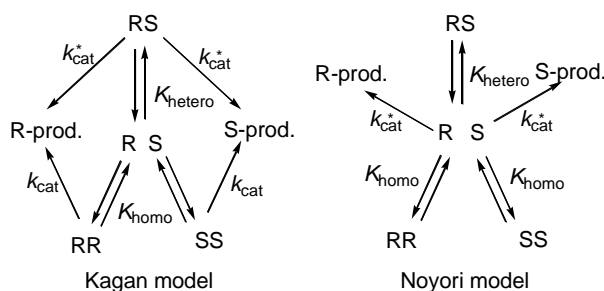
Scheme 7. Kagan's and Noyori's NLE models [84].
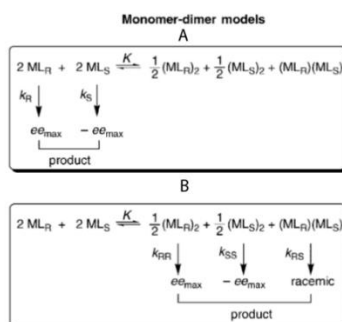
Scheme 8. Monomer–dimer models: (**A**) monomer is a catalyst, (**B**) dimer is a catalyst.

The explanation for the single NLE in the form of the rate constants balance in the models is complex though not yet comprehensive. The proposed models do not take into account all reaction parameters that influence this effect. Indeed, the remarkable (–)- NLE in a reaction of diethylzinc addition to benzaldehyde (5) over (*S*)- and (*R*)-fenchols **6** (X=H or CH$_3$) changes with respect to a linear relationship over (*S*)/(*R*) fenchols with X=SMe$_3$ and X-t-Bu [63] (Scheme 9).

6 (racemic mixture)
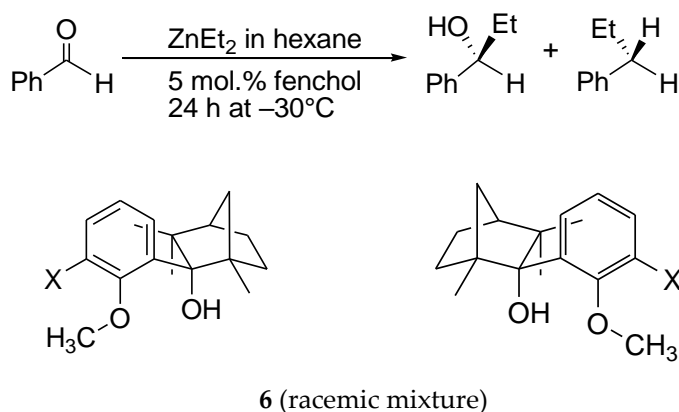
Scheme 9. Diethylzinc addition to benzaldehyde over fenchol **6** rac.

Chen et al. [88] observed a NLE dependence on the substrate in the reaction of diethylzinc addition over chiral auxiliaries **7** and **8**. (Scheme 10).

R,R-8, *S,S*-8, *R,S*-8
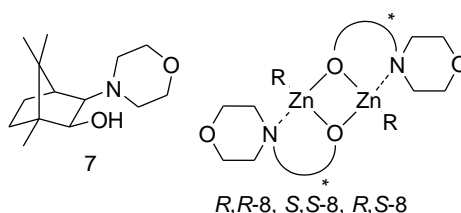
Scheme 10. Diethylzinc addition to benzaldehyde in the presence of chiral monomer **7**, dimer **8** and **8rac** ligands.

Electron-donating substituents affect the positive NLE to a greater extent than electron-withdrawing substituents in aromatic ring of aldehydes. Kagan and Noyori models do not take this effect in consideration. The S-shaped curves of NLE (multi-shape NLE, Figure 7) add complexity to the understanding of this phenomenon (e.g., [89,90]). Positive and negative NLE maxima of the curves correspond approximately to 25% and 75% optical purity of chiral auxiliaries. Therefore, the internal relationship between the maxima and corresponding minima on the curves of Wallach's dependence is quite possible (Figure 1a,b).

Kitamura, Noyori et al. [81,82] observed an extremely marked (+)- NLE in the reaction of diethylzinc addition over the catalyst derived from amino alcohol DAIB (**9**) (see Scheme 11).
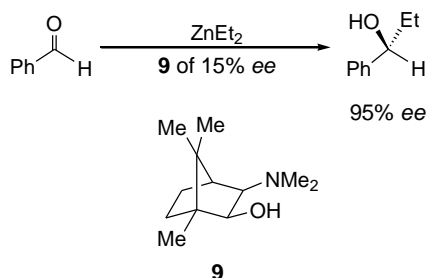
Scheme 11. Diethylzinc addition over ligand **9**.

Only the Soai reaction exceeds many catalytic reactions in terms of the enantioenrichment of the product relative to the catalyst during one reaction. Diisopropylzinc addition to pyrimidine) carbaldehydes (Soai reaction) is a well-studied cryptochiral reaction [91–96] (Scheme 12).

Scheme 12. Soai reaction.

The expected *ee*% of the product is four orders of magnitude less than in the experiment [96]. The Soai reaction mechanism (asymmetric autocatalysis, asymmetric autoamplification, and asymmetric autoinduction) is discussed [91–98].

The well-known term "asymmetric induction" is sometimes, though rarely, replaced by "chiral induction", which is not correct. There are many examples to prove that reactions of monofunctional substrates (e.g., hydrogenation of acetophenone, benzaldehyde, etc.) in the presence of C_2-symmetric chiral catalysts do not proceed enantioselectively [99–106]. It is a result of the single-point coordination of the substrate with the C_2-symmetric chiral catalyst (chiral induction). Where the substrate is coordinated by two or three groups (three-point coordination, e.g., in hydrogenation of amino acid precursors), catalyst's C_2-symmetry is lost at the stage of the catalyst-substrate intermediate complex; high enantioselectivity is provided. The reaction of deracemization (Scheme 13) exemplifies a possible presence both of asymmetric and of chiral (not leading to enantioselectivity) induction in one reaction [107].

AAL	*ee*(%)
KBr	> 99
KCl	< 2

Scheme 13. Catalytic reaction of deracemization. AAL—achiral addition ligand.

In heterogeneous catalysis, asymmetric reactions occur not in the catalyst volume but on its surface (Scheme 14) [108–124]. Therefore, asymmetric induction is determined by chiral adsorption of prochiral substrates. Chiral adsorption, in turn, depends on chiral compounds (including C_2-symmetric) adsorbed on the surface prior to the asymmetric reaction (modifiers).

Chiral structures on the surface can be created by adsorption of achiral molecules [108–111]. However, asymmetric reactions (e.g., hydrogenation of prochiral substrates on metals) occur on the surface of the catalyst in the presence of adsorbed chiral compounds (modifiers) [112–114]. In this case, the chiral adsorption of the prochiral substrate proceeds with the formation of an intermediate complex (substrate—metal atom (or a cluster of atoms)-modifier) [112–114].

Scheme 14. Mirror symmetry of planar molecules on a surface.

Two approaches to study the mechanism of asymmetric heterogeneous catalysis are possible; insight from modifier's chiral structures on catalyst surface [112–124] and insight from asymmetric induction mechanism in intermediate complex on the surface [99–106].

According to the first approach, a chiral modifier creates a hierarchical cascade of phases on the metal surface (Scheme 15) [115–119].
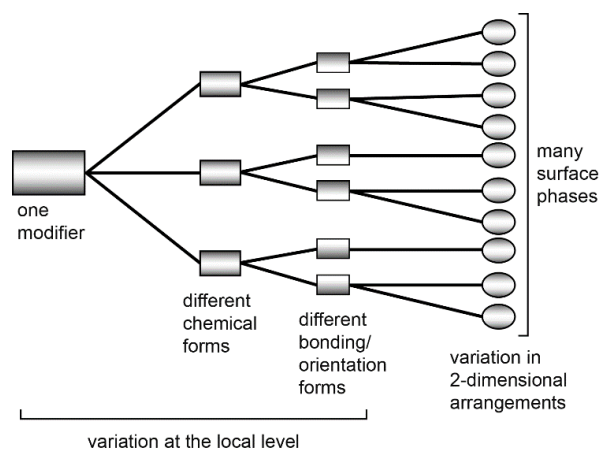
Scheme 15. Schematic cascade of organic molecule phases on a particular surface.

This scheme indicates the diversity of adsorption forms of modifier on the surface of the catalyst.

Raney nickel-(R,R)-tartrate complex as catalyst in prochiral ketones hydrogenation is the most enantioselective catalytic system [90]. Therefore, this system was studied as (R,R)-tartrate on Ni surface at different temperatures (Figure 8) [115–119].
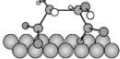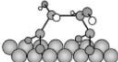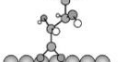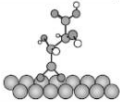

Figure 8. Phase diagram of (R,R)-tartrate on Ni(110).

The Figure 8 illustrates the variety of forms of *(R,R)*-tartrate adsorption on the surface of Ni catalyst at various temperatures. This data corresponds to the difference in enantioselectivity of this catalyst at different temperatures [115–119]. It is possible that the diversity of modifier adsorption forms (Scheme 15 and Figure 8) leads to a variety of asymmetric induction mechanisms. These data apparently explain the lower average enantioselectivity of heterogeneous catalysts [112–114] compared to homogeneous.

However, the surface of the metal catalyst is not perfectly flat. Moreover, the most catalytically active zones of the catalyst are surface defects (peaks, edges, pits, etc.) [112–114]. They are apparently the most enantioselective zones of the catalyst modified with chiral compounds. Therefore, a second approach to the study of heterogeneous asymmetric catalysis can also be fruitful. For example, conformation of diketone in homogeneous heteroligand complex (acetylacetone–metal–chiral amino acid) can imitate the conformation of this substrate on the surface of the modified catalyst (Figure 8) [99–106]. Aromatic amino acids (tryptophane, phenylalanine and tyrosine) are a simple and convenient modifier to create chelate complexes and to imitate intermediate complexes on the metal surface. The planar arrangement on surface of this modifier can be provided by → * bond of aromatic ring of the amino acid. As it can be seen from the Figure 9 the preferred λ or δ conformation of diketone (known from CD-spectra) leads to a preferred attack 2H from metal surface.
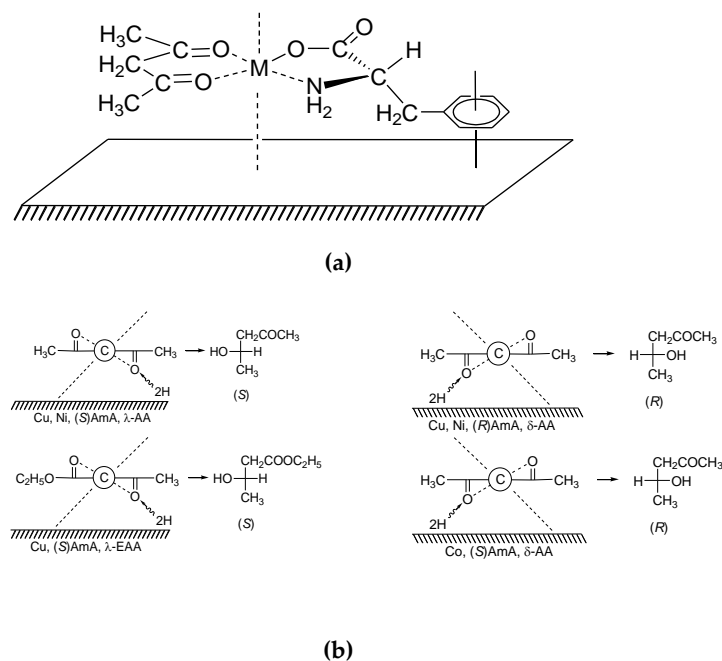

(a)

(b)

Figure 9. (**a**) The plausible structure of intermediate complex; (**b**) the mechanism of enantioselective hydrogenation of acetylacetone and ethyl acetoacetate (AA and EAA) over Cu, Ni and Co catalysts modifi*e*d by *(S)*- and *(R)*-amino acids (AmA).

It can be seen from schematic structure of intermediate complex, conformation λ of AA (EAA) correspond to (S)- product whereas conformation δ teads to (R)- product [99–106]. Therefore, it is possible that asymmetric induction occurs in such asymmetric intermediate complex.

5. Possible Physical Background of Wallach's Rule and Similar Phenomena

Apart from the capability to change physical properties (density, melting point, solubility), the racemate has a special property that can be interpreted as "chiral recognition" [125]. This original term reflects an impression that an enantiomer of one sign selects an enantiomer of another sign from the mixture of both enantiomers. It is formally completely analogous to mirror reflection. From this viewpoint, the mirror performs an action, i.e., reflection, which is similar to "recognition" of one

enantiomer by enantiomer of another chirality sign. Does this action have a physical entity or physical essentials? In other words, does a similar action occur in nature as an artifact? Examples found in nature may help verify the hypothesis on the physical significance of mirror reflection. First of all, these are encountered as defects in linear helical macromolecules. The formation of a helical structure of one sign of chirality can sometimes be accompanied by a change in the chirality sign of the helix without bond breaking.

G. Singh et al. [126] observed that dipoles of nanocrystals of magnetite Fe_3O_4 self-assembled into helical superstructures in the magnetic field. In accordance with the theoretical concepts of P. Curie et al. [127,128], it can be assumed that only a combination of the magnetic field with another field (electrical [98] or gravitational can be an asymmetric inductor of these chiral superstructures formation. Among a variety of Fe_3O_4 superstructures with SEM images (Figure 10; of special attention is Figure 10c,d). As seen, the linear right-handed helical structure of the nanocrystal superstructure in the "defective" area is replaced by the left-handed helix.
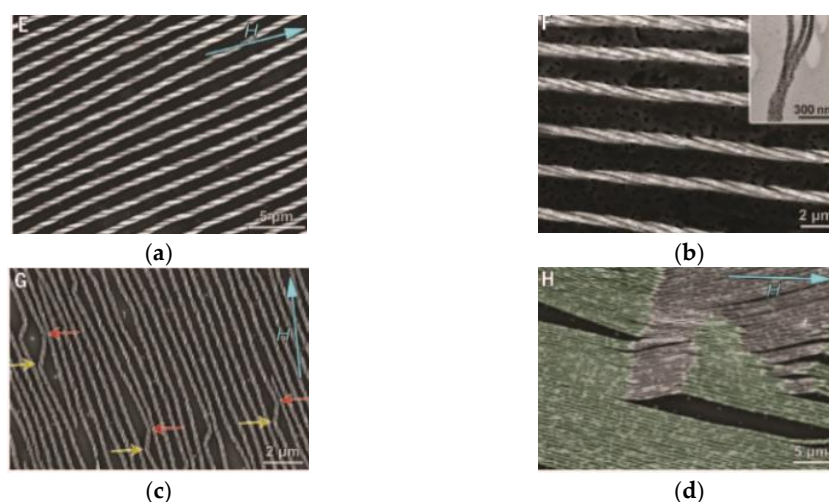

(a)   (b)   (c)   (d)

Figure 10. The array of Fe_3O_4 nanocrystal superstructures: (**a**) single handedness helix, (**b**) triple helix and (**c,d**) "defects".

Mirror symmetry points ("defects") are shown by arrows. The "defects" and the angle between linear macrostructure fragments of opposite chirality signs (~130°) in the mirror symmetry points strikingly resemble theoretical points calculated for other chiral macrostructures (Figure 11) [129,130]. Indeed, the calculated data show that the inversion of the right-handed helical conformation into the left-handed one in polyisocyanates during polymerization occurs with a change in the linear direction of the polymer chain at the angle of 130° [129,130].
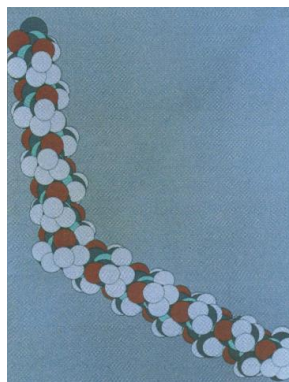

Figure 11. Calculated mirror symmetry point of the helical symmetry reversal (junction) of poly(ethyl)isocyanate.

Similar data are available for other nanostructures. Studying boron nitride (BN), Celik-Aktas watched regular dark and bright spots on the side walls of a BN nanotube (transmission electron microscopy). Basing on that, the authors [131–133] suggested a double-helix structural model. A kink at a 130° angle of one of the threads of the BN nanotubes in the TEM image can be explained by a similar effect. The possible right-handed helix structure changed into a structure with the opposite chirality sign (Figure 10c,d) (indicated by an arrow) with the angle of ~130° as well.

Of great interest is a difference in the physics of crystallization according to Wallach and crystallization of a mixture of well-faceted enantiomorphic crystals (conglomerate), in particular *l*- and *d*-crystals of $NiBr_2((R,R)$–dpcp$)\cdot CH_2Cl_2$ and $NiBr_2((S,S)$–dpcp$)\cdot CH_2Cl_2$ [29]. Indeed, there is an obvious difference between these crystallizations. Wallach's rule is fulfilled on the basis of mutual attraction of enantiomers having different chirality signs which crystallize as a racemate, while a conglomerate is formed during co-crystallization of enantiomers of the same sign (attraction of enantiomers of the same sign) and repulsion of enantiomers of different signs.

A widely used physical phenomenon that combines attraction and repulsion is the interaction of magnetic S/N poles. In contrast to natural crystallization of molecules, S/S- and N/N- repulsion of the magnetic poles (magnetic levitation) requires a certain orientation of magnetic fields.

A chiral molecule is sometimes compared to a turn of a helix twisted to the right (*P*) or left (*M*). We tried to compare the chiral molecule with the right-handed or left-handed coil of the helix through which electric current passes. If the coil structure simulates a chiral molecule, the current direction models the polarizability direction of the chiral molecule (Figure 12).
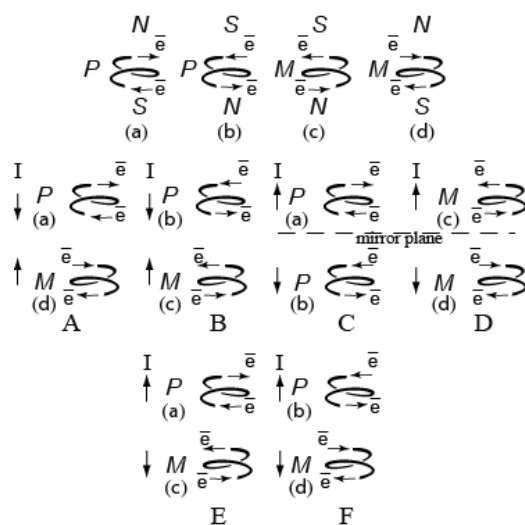

Figure 12. The direction of impulse (I) of the interaction of magnetic fields of two individual coils (*P*—right-handed, *M*—left-handed) depending on the direction of current: A,B—attraction; C–F—repulsion.

Figure 12 shows combinations of two coils of a different chirality sign and different direction of current. A and B pairs (represent attraction) model crystallization that proceeds in compliance with Wallach's rule, while two pairs of C and D coils representing repulsion simulate separate crystallization of *l*- and *d*-crystals. The pairs of C and D coils differ in both the sign of chirality and the direction of current. Given that a comparison of chiral coils magnetism and crystallization of chiral molecules is valid, these pairs could simulate crystallization of *l*- and *d*-crystals (Figure 3). Postulating the equal contribution of all pairs to the total balance, the A and B pairs (racemates) account for one-third (33.3%), whereas the portion of C,D,E,F pairs is two-thirds (~66.7%). Thus, four pairs of coils C–F represent the contribution of repulsion of enantiomers with different chirality signs, that is they represent crystallization of the conglomerate of *l*- and *d*-crystals. Therefore, maximum optical purity should not exceed 66–67%. This forecast is in good agreement with the experiment (Table 1).

It should be noted that such comparison is rather formal. It is currently considered that the magnetic field has only the axial structure. Preservation of the helical structure of the coil with current in the magnetic field generated by it is not discussed in theoretical physics. However, the experimental detection of the helical structure of the Fe_3O_4 [126] nanocrystals array (Figure 10) after crystallization in the magnetic field brings about doubts regarding the categorical exclusion of the helical structure of the magnetic field or one of its field levels.

Similar views can also be found in explaining the physical basis of asymmetric catalysis. For example, a new theory of asymmetric catalysis has been developed by Wang [134–137]. He suggests that chirality (helical asymmetry, chiral molecular recognition and induction) depends on electronic repulsion of substituents (Scheme 16). The theory assumes that molecular helicity on the base of electronic repulsion in asymmetric catalyst must be matched to molecular helicity of catalyst–substrate intermediate state (Scheme 17) [138,139].
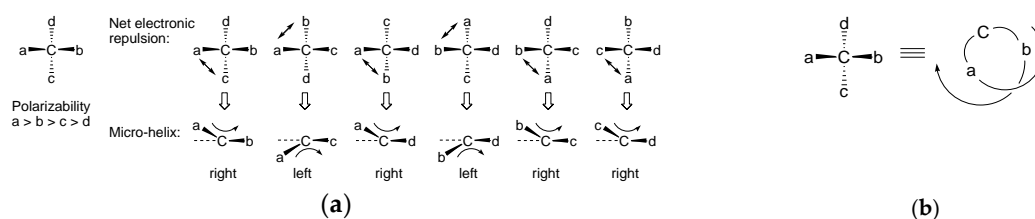
Scheme 16. (**a**) Helical structures with a group polarizability sequence a > b > c > d; (**b**) right-handed helical deformation on the basis of first structure only.
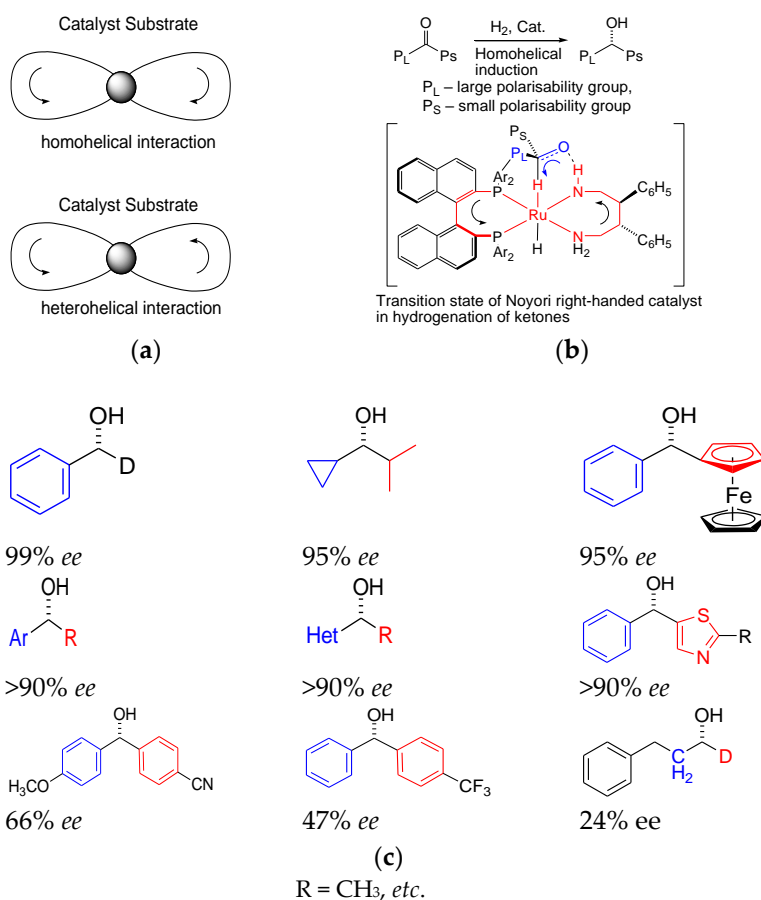
Scheme 17. (**a**) Homohelical and heterohelical electronic interaction in transition state, (**b**) ketone hydrogenation over corresponding homohelical transition state, (**c**) the row of ketone substituents polarizability difference and hydrogenation enantioselectivity (*ee*%).

Therefore, the right-handed catalyst in the hydrogenation reaction will lead to a more enantiopure product, with substrates forming right-handed transition states (homohelical interaction). In the case of Sharpless asymmetric dihydroxylation (AD) reactions (Scheme 18a) the row of polarizability 13–17 (Scheme 18b) take place [140].
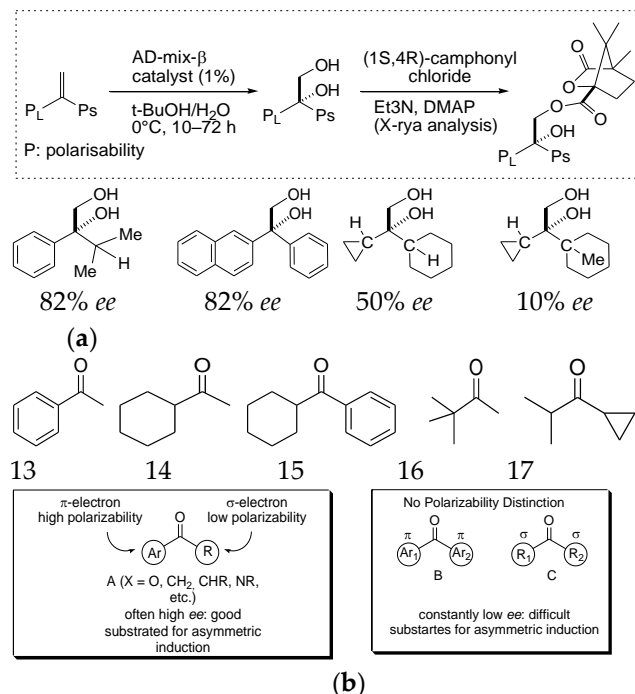
Scheme 18. (**a**) Polarizability—controlled Sharpless AD process, (**b**) asymmetric induction row with polarizability—based rationale.
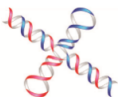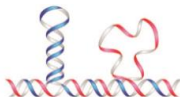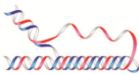
Thus, the virtual coils with current symbolizing attraction and repulsion (Figure 12) and the helical structures of virtual coil of polarizability sequence (a > b >> d) in catalyst and substrate (Schemes 17 and 18) may have some common basis related to polarizability.

6. B–Z DNA Transition

The B–Z DNA transition is of great interest for the elucidation of a physical basis or physical sense of mirror reflection (with the replacement of the right by the left and alternatively). The junction point of the right-handed double helix of canonical B-DNA with the opposite left-handed double helix of Z-DNA is biologically important and relatively well researched as a reversal point of helical symmetry. Despite its seemingly stable structure, the double helix of DNA molecule is a rather unstable structure for external impact. Indeed, more than one hundred oxidative breakdowns of DNA are known. Conformational damage of the DNA molecule (Table 3) [141,142] leads to genetic instability and genetic diseases [141–148]. The B-Z DNA transition is among the most severe damage kinds. Such conversion with two inversion points is shown in Table 3 as a linear segment of the DNA molecule (B–Z junction) [141,142].

Nucleobase pairs in the Z DNA fragment are directed opposite from those in the B-DNA fragment [149]. Crystalline B- and Z-DNA fragments are connected linearly (at the junction points) only with one base pair breaking and extrusion of base ends (Figure 13). So linear binding of B- and Z-DNA fragments in the DNA molecule in the genome should occur with great steric hindrances [149]. It is difficult to explain the linear combination of B- and Z- DNA fragments which is even "highly improbable from a physicochemical viewpoint" [149–154].

Table 3. Non-B DNA conformation.

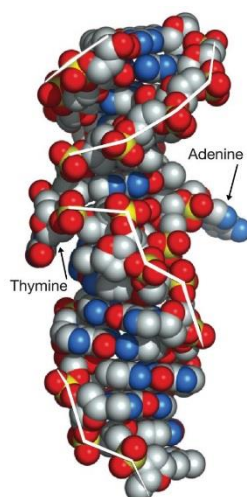| Name	Conformation	Name	Conformation
Cruciform		Slipped (hairpin) structures	
Triplex		Left-handed Z-DNA	

Figure 13. Van der Waals view of the B–Z DNA junction.

It should also be noted that the Z-DNA segment in the genome is loaded with a large number of B-DNA fragments of opposite configuration. Therefore, the B–Z DNA transition does not occur spontaneously (as in the case of the phenomena discussed above Figure 10). The B–Z DNA reversal demands energy to create the B/Z junction [150–153]. A free energy difference is about 0.9 kcal/mol per dinucleotide unit to induce the B–Z DNA transition [155,156]. Some researchers [157] believe that this process needs an intermediate stage (hypotetic *S*-DNA with the right-handed double helix structure). Thus, it can be assumed that the B/Z DNA junction emerges under the influence of an external chiral inductor or chiral doping.

The B–Z DNA transition is facilitated by changing the salt environment [158]. Therefore, a mixture of ions (particularly of cations) greatly affects this transition. This effect can be largely explained by a decrease in the interaction between oppositely positioned phosphate groups in B- and Z-DNA. Indeed, these groups get closer to each other in Z-DNA compared with B-DNA (7.7 in Z-DNA and 11.7 Å in B-DNA) [159–161]. Therefore, negatively charged phosphate groups of B- and Z-DNA fragments interact with surrounding ions in a different manner. It is interesting that solvents changing the dielectric constant of water stabilize Z-DNA to a greater extent [162–169]. Additionally, metal complexes differently affect the B-Z DNA transition [170–173]. However, compounds with very strong chiral induction have the highest effect. Given that, helicene helix molecule exerts the most significant impact on the B-Z DNA transition. Chiral hexahelicene is known to have huge "rotational power" (immense chiral field) in circular dichroism (CD) spectra. Xu et al. first reported structural selectivity of helicene 1 in the action on DNA [174].

The CD spectra of the (P) –helicene/Z-DNA mixture (d(CGCm8GCG)$_2$ as a model of Z-DNA) shows the 70% intensity decrease. Whereas no change occurs in the (*P*)-1/B-DNA mixture (d(CGCGCG) as a model of B-DNA). No discrimination is observed in the CD spectra of the (M)-helicene/B-DNA and (M)-helicene/Z-DNA mixture. The decrease in intensity here is as low as 20%.

This observation brings us to a fundamentally important conclusion about the possibility of an external chiral effect on DNA. This influence on the chiral DNA conformation may be ascribed to a greater degree of the helicene chiral field. Can a physical factor (field or radiation) affect the chiral conformation of DNA?

An analysis of impact of electromagnetic fields on DNA shows that stable magnetic or electric fields do not affect DNA. Apparently, this can be explained by the fact that these stable fields exist on Earth. DNA has been evolving for billion years in the presence of stable magnetic or electric fields. Therefore, the DNA molecule as the most important molecule in the genome probably has protection mechanisms against damage from stable electromagnetic fields. There are certain repair mechanisms in a living cell such as "nucleotide excision on repair", "mismatch repair" and so on [175]. It is possible that the analogous protection mechanism exists to counteract stable electromagnetic fields and that the DNA molecule is not sensitive to stable electromagnetic fields.

However, the situation is completely different in the presence of high or low frequency electromagnetic fields. These exert a genotoxic effect [176,177], along with DNA double-strand breaks [178–182], and some other similar effects [183–189]. Indeed, variable electromagnetic fields, including those of low frequency, do not exist on Earth. Perhaps, this is why the DNA molecule has no protection against them and is vulnerable in their presence.

Thus, hypothetical breaking of the energy barrier of the B/Z DNA junction can take place in two stages. An external chiral inductor, acting as a trigger, can send the first impulse to clear the barrier [43]. At the second stage, the B/Z DNA junction receives an energy advantage by analogy with Wallach's rule (a denser arrangement of phosphate groups [161] in the "racemic" structure of B–Z DNA).

Similar inversion points also occur in simpler linear structures. Areas of change in the sign of helicity *M/P* (or *P/M*) may occur also between superstructures from achiral molecules in chiral domains [43]. Tomsett et al. [190] showed that a screw-sense reversal (inversion points) was noticed in oligomere molecules. This "tendril perversion" was "trapped within a fragment of a helical oligoamide foldamer of the achiral quaternary amino acid 2-aminoisobutyric acid". These chirality inversion points (*M/P*-point) were monitored by NMR, CD-spectra, X-ray crystallography, Raman spectroscopy, and modelled computationally.

Hence, there is probably an energetic advantage of 50%:50% (L/D) structures in the LC phase and (L/D) chirality inversion points within the oligomer molecule boundaries or just in the double helix of the DNA molecule. A similar trend exists in spontaneous reactions (Figure 10). Therefore, "racemic" composites, chirality inversion points within the limits of a linear structure and Wallach's rule have much in common. Is it possible that they have a common physical basis?

The Dzhanibekov effect may also be responsible for the external chiral inductor's influence on the appearance of inversion points.

7. Chirality Inversion Points or Mirror Image Effect of Moving Objects

Astronaut Dzhanibekov [191] was the first to view changing of the uniform motion of an object in zero gravity. He observed that a hex nut (jumped off the thread), as it moved in zero gravity (after about 20 rotations around the axis), made a somersault and continued to move with rotation. The sense of rotation of this object before and after the somersault was actually mirrored.

It is known that the Earth's magnetic field changes its polarity every half million years on average [192,193]. The last change took place about 750 thousand years ago. Assumingly, the movement of rotating ions in solution may have similar effects (Figure 14).

A conglomerate (50%/50%) of $NaClO_3$ crystals (see Scheme 1) is a possible consequence of this effect in the absence of stirring. Taking into account the weight of the discussed objects, the somersault frequency will be inversely proportional to the object mass. Thus, the inversion of the object moving with mirror-symmetric tumbling occurs also in the case of linear rotational motion. It is expressed in the periodic change of axial rotation of the object (with a somersault). What makes a moving and rotating object fulfill a roll/inversion with the helical trajectory change to the mirror opposite? Whether a cause

of this mirror symmetry inversion can be related to the L/D inversion pattern of helical macromolecules and similar effects?
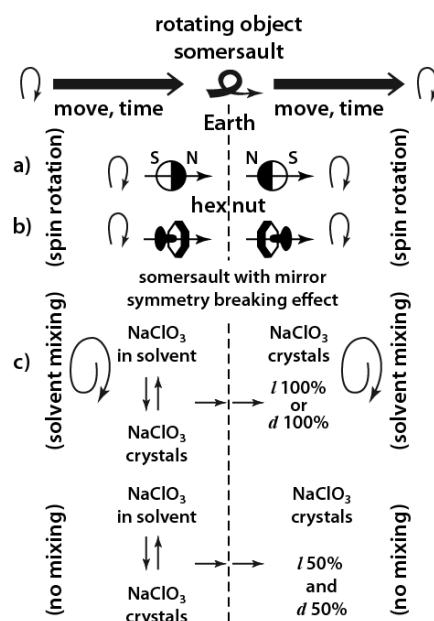

Figure 14. Possible influence of the Dzhanibekov effect on mirror symmetry of moving objects.

8. Chiral Trajectories of Moving Objects as an External Chiral Inductor

The origin of life was actually determined by the nature's choice of the configuration series: L-amino acids and D-sugars. This configuration relationship of amino acids and monosaccharides was selected from the four possible (D–D, L–L, D–L, and L–D). A reason for the choice has been still under discussion [194–205]. "A possible basis for such a row of configurations can be right-handed helix conformations (*P*) of important biomacromolecules" (Scheme 19) [66,192,193].

right-handed helix (*P*- helix or -helix) of polypeptides

right-handed double (*P*) helix of DNA

right-handed triple (*P*) helix formed by important polyglucanes
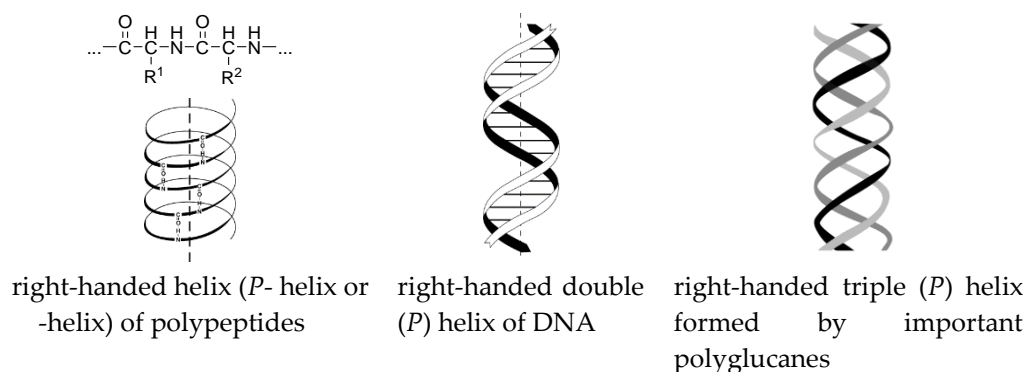
Scheme 19. Important biomacromolecules.

All these vital *P*-macromolecules only consist of L-amino acids and D-sugars. The choice of the *P*-macromolecule configuration depends on the external chiral inductor. Electromagnetic fields, circularly polarized light, plasma torch of meteorite impact, solar irradiation, parity violation energy difference, and similar factors can act as an external chiral inductor [66,67]. Hypothetical gravity impact can be a possible physical inductor acting as a chirality trigger [66,67]. A basis for this assumption is Barron's concept [206] of true and false chirality. The combined gravitational field of moving space bodies surrounding Earth creates a chiral gravitational environment on Earth (Figure 15).

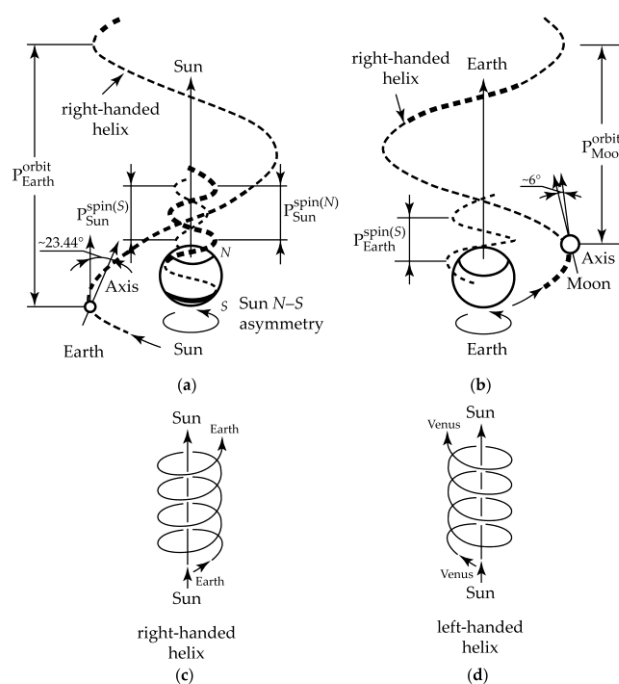**Figure 15.** Helical trajectories of the joint movement (orbital and spin rotation) (**a**,**c**) Sun-Earth, (**b**) Earth–Moon, and (**d**) Sun–Venus. Pitches (P) of the helices: PE_{spin} = 1 day, PE_{orbit} = 1 year, PM_{spin} = PM_{orbit} = 1 lunar (sunderic) month, $P_{Sun}{}^{spin(N)}$ = $P_{Sun}{}^{spin(S)}$ = ~38 Earth's days (near the polar caps of Sun). Rotation of Sun around the axis tilted 82°45' to the plane of the Earth's orbit occurs in the same direction as spin rotation of Earth (counterclockwise).

A striking resemblance is observed between the Earth's right-handed rotation (spin) near the Moon, the right-handed Earth's orbital trajectory moving around the Sun, and the right-handed helix symmetry of molecules of life such as polypeptides, DNA, and polyglucanes (Scheme 19). He et al. were the first to note this relation [207–210]. The Solar system moves also along the right-handed trajectory in the Milky Way galaxy [211–215]. However, the Galaxy itself has a more symmetrical structure similar to a "top-bottom" double snail [211–215]. There is a similarity between the Galaxy structure and a meso-structure (inner racemate).

Indeed, "the mirror symmetry plane divides the right-handed (*P*-snail) field and the left-handed (*M*-snail) field of the Galaxy" [211–215]. Because the Solar system is located in the *P*-snail field, the Sun, Earth and other planets move identically (clockwise), with the exception of Venus.

The effect of gravity on a chemical reaction is rather strange and unusual for a chemist. Indeed, experimental verification of gravity impact on chemical reactions is feasible only in a space flight. In addition, a possible gravity effect on unstable chemical reactions becomes obvious after the discovery of gravitational waves [216]. However, gravity research in chemistry began with the most stable reactions such as nuclear decay. Indeed, many scientists believe that nuclear decay is generally not applicable to external physical inductors. Fischbach et al. [217–221] watched Cs decay on board the Messenger during its flight to Mercury. Additionally, the authors observed Mn decay during the Solar flare on 13 December 2006 [67].

The idea was to demonstrate the limits of a possible correlation between ^{54}Mn, ^{32}Si, ^{36}Cl, and ^{226}Ra nuclear decay rates and the Messenger–Sun distance. The positive interpretation of these data on the effect of gravity on the nuclear decay rate has opponents [222,223]. No doubt, the gravity effect on reactions less stable than nuclear decay will be great. We should also take into account the doubtlessly chiral gradient of gravity and millions of years of its stable engagement in the formation of biologically active molecules.

Additional data on asymmetry of the gravitational field as a result of right-handed trajectories (see Figure 15) are obtained from the observation of North-South solar asymmetry and anisotropy of cosmic rays over the solar polar caps [224–226].

The conclusion on the influence of chiral gravity on chemical reactions leads to another very important finding [43]. The chiral gravity effect depending on moon tides on Earth initiates a stable level of the B–Z DNA transition. B $\leftrightarrow$ Z DNA equilibrium may appear damaged in the other gravity conditions. Therefore, extensively publicized intentions of some politicians to set up lunar settlements in the future will only become realistic unless robots are used. Life in lunar settlements in the conditions of stable gravity (exported from Earth on Moon) and zero magnetic field on Moon ($P_{Moonorbit}$ = 1 lunar (sunderic) month, in other words, Moon faces Earth with only one side) can be dangerous [43] for biologic objects (as well as space flights in zero gravity)

9. External or Internal Chiral Inductors. Chiral or Racemic Water Flows

An accident at the Sayano-Shushenskaya HPP (Russia) on 17 August 2009 is the most mysterious event in the history of hydropower plants [227]. The fact of breaking dowels of the turbine top plate and pushing the multi-ton structure upwards contradicts all principles of turbine operation. There is an opposite expert opinion. The cause of the accident according to the official version was a violation of the turbine operation rules. All responsibility was passed on the HPP personnel—the so-called "human factor". However, it is known that the vibrations of the hydroturbine unit at the Sayano-Shushenskaya HPP slightly differed from the known vibrations. It is unlikely that these could damage two-thirds of 80 dowels that fixed the generating unit. Now there is every reason to suppose that it was not the human factor that was responsible for the accident. Indeed, the inspection reported the breakage of some of those 80 dowels due to 35% fatigue, which was admitted as the main cause of the accident. By evaluation, the force that broke loose almost a third of the 80 dowels had to be about 6700 tons. If added to the weight of the pushed-out part of the unit (the turbine wheel, turbine cover and generator rotor, total weight 1687 tons), remarkably, the total force is 8400 tons. Here you need to add the force that led to damage of two-thirds 80 dowels. Therefore, the total force that caused the accident (Figure 16) had to exceed 10,000 ton.

Figure 16. Pushing the multi-ton turbine assembly up during the Sayano-Shushenskaya HPP accident on August 17 2009.

The maximum turbine unit vibration amplitude before the accident is known to be 1500 μm. Under such conditions, an unfixed 8000-ton unit would not budge [227]. So, all attempts to explain this accident stemming conventional concepts were failing [227–230].

Let us assume that the dynamic conditions for the accident could have been created because of the increased water flux density in the water conduit (Figure 17). A possible cause of the accident could be a sudden abnormal increase in pressure of water entering the turbine through the conduit. It is known that helical movement of water leads to an increase in pressure and range of the water stream when fighting fires. To create a spiral flow of water, such designs are a special additional turn of the pipe. However, helical movement in the HPP could be created spontaneously. This motion could be created and amplified by resonance with an external inductor (for example the Earth's rotation).
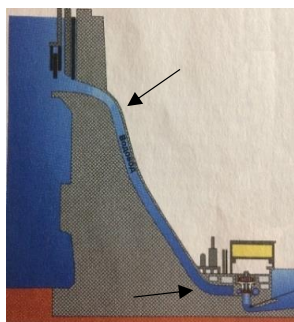
Figure 17. Schematic image of the water conduct at the Sayano-Shushenskaya HPP.

It is also possible, that the casual structure of the water conduit created an angle of the direction of water flow close to 130° (Figure 17, shown by arrows). The sequence of this change in flow direction could be a change in helix chirality similar to the phenomena that are reflected in the Figures 13–15 with inversion points 130°. This change could further increase water pressure according to the Wallach's rule. The inversion point could also stabilize helical configuration of the water flow coming to the turbine If. this helix configuration does not match the helix configuration of turbine (Figure 18), this could have fatal consequences.
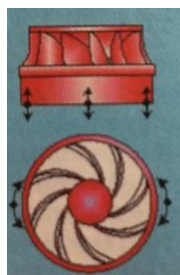

Figure 18. Hydroturbine structure.

It should be emphasized that proposed hypothesis is based on a possible increase in the density of water in conduit of hydroelectric power plant.

It is based only on external similarity of possible chiral water flows and chiral macromolecules. A group of technical experts questioning the official explanation of the causes of the accident suggests a hypothetical external factor. Chiral water flows can be initiated by external chiral factors including stochastic factors that are difficult to model.

The above mentioned group of experts emphasized that accidents of this kind (not as tragic as in the Sayano-Shshenskaya hydroelectric power station) occurred at other high-pressure stations around the world. Therefore, the reason may be similar as well.

10. Mirror Symmetry Effect in Biology

It is known that two organelles are located near each ear of a human (Figure 19). Apart from other functions, this paired organ performs acts as the vestibular apparatus. These symmetrically located organelles have snail-shaped fragments with the right- and left–handed structure. In fact, these snails are an object and its mirror image. Such an arrangement should have its internal sense for orientation.

Orientation with the help of the vestibular apparatus is possible when information from left-handed and right-handed snails is detected. Most likely, a chiral or asymmetric detector of the human body can implement this control correctly. Apparently this function can be performed by the human brain. The human brain is characterized by bilateral symmetry of two hemispheres which are interconnect white matter tissue. The left and right hemispheres differ between themselves in size and weight within small limits. The differences from person to person are in different symmetry of the brain cortex

of two hemispheres with each other. The brain cortex topography of two hemispheres changes from mirror symmetric to completely asymmetric (Figure 20) [231–236].
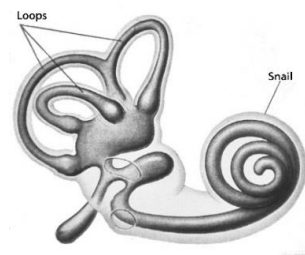

Figure 19. Left-handed snail organelle of human vestibular system.

(**a**)   (**b**)
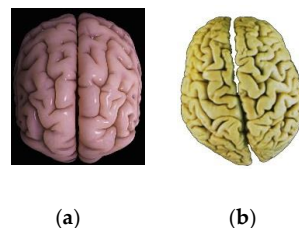
Figure 20. Structure of brain cortex hemispheres: (**a**) symmetric (plane of symmetry), (**b**) asymmetric.

However, the brain with a plane of symmetry between hemispheres does not allow to estimate mirror symmetry of object. The symmetry of the right and left is result of option involving C_2 axis of symmetry. A symmetrical brain would consider the left and right as symmetrical. Indeed, we belong to the bilateral group of species whose body plan is essentially symmetrical. Therefore, we need a chiral or asymmetric organ that can evaluate the right and left surroundings [237]. For example, a person looking at himself in mirror can understand that the ring is on his right hand, although in a mirror image this ring is on his left hand.

It is interesting that some correlation between the symmetry–asymmetry of the cerebral cortex and illiteracy/literacy of the observed person was popular in the late 19th century.

Modern tomographic studies show that a decision making process involves various brain areas. These areas may even compete for decisions. However, it is believed that the frontal lateral cortex plays a major role in decision-making. Therefore, symmetry of the cortex, probably, also impacts the information evaluation and final decision making. Figure 21, demonstrates how nature strives to avoid brain mirror symmetry even in its functions [231–236]. Mirror symmetry is retained only in cognitive analysis (see, for example, mirror neurons phenomenon).

Figure 21. Brain lateralization.

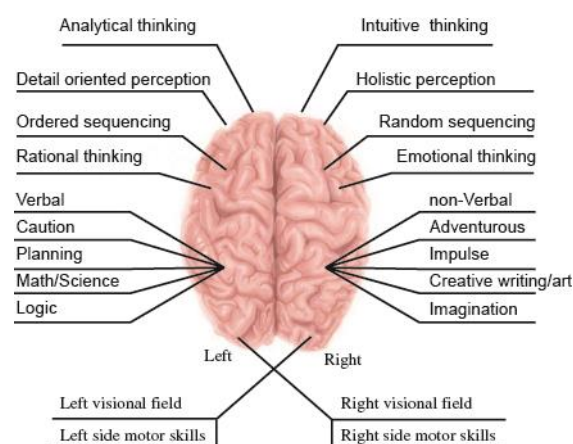Therefore, brain performs this function as an asymmetric body. The left hemisphere is leading in the intellectual function, while the right hemisphere is responsible for mental and emotional functions. Moreover, motor functions are distributed in the hemispheres from the left hemisphere to the right side of the body and alternatively. Thus, the sensory response of the brain is devoid of symmetry elements, i.e., it is asymmetric.

It is interesting that there is a problem of righties and lefties. We are almost all right-handed [238–240], which is often a source of prejudice against about 12% left-handed. Fossil sources suggest that even Neanderthals were righties, perhaps in the same proportion as modern humans [240]. Modern right-handed people perceive left-handed people not as defective but as an interesting difference from "their beloved ones". However, there is a physical base of difference between left and right that causes emotional reaction of human. This reaction is associated with the participation of "mirror neurons" in the brain (Figure 22).. When we see manifestation of a positive emotion, such as smile, we also feel a similar emotion. It was discovered that the reproduction of these emotions is controlled by neurons with new structure [241–244].
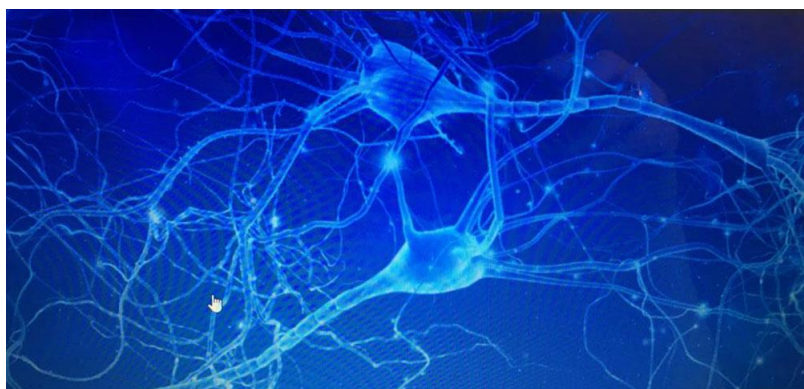

Figure 22. "Mirror neurons" structure.

Synchronous perception of this emotion is maximal when we are strictly vis-à-vis another person. Therefore, these neurons we called "mirror neurons" in full accordance with their functions. Indeed, it is entirely possible that this synchronism estimated by the brain when it evaluates the right and left. In this case, the right and left are evaluated by the same "mirror neurons" while the motor function of the right and left sides of the body are controlled by ordinary neurons of different hemispheres of the brain. The brain choice of special neurons for the analysis of the right and left in the emotional plane. These neurons connected with abstract thinking. This assumption is based on the observation that these same "mirror neurons" are involved in the learning process.

Another scenario involves the participation of mirror symmetry effect to act on the mirror neurons. The effect of mirror symmetry is based on the assumption that there are not only structural but also physical difference between the right, left, and their mixture. The examples discussed in this review testify also to this. The physical basis of the right and left (between vis-à-vis exposed persons) as similar effect can act like a trigger for operation on the same "mirror" neurons.

11. Mirror Symmetry Effect in Physics

An experiment conducted by the Baryon Antibaryon Symmetry Experiment group of the European Centre for Nuclear Research (CERN) has demonstrated that magnetic moments of proton and anti-proton differ only in signs, while they are the same with record accuracy [245–247] in the numerical expression. Basically, they are equal. This confirms that the "material" proton and "anti-material" anti-proton are symmetric particles or mirror images of each other. A similar situation is possible for "material" elementary particles—neutrons, protons, electrons, etc.—and anti-neutrons, anti-protons (as it was observed experimentally), anti-electrons, etc. However, this scientific viewpoint includes

a striking paradox. Indeed, matter and anti-matter have no advantage over each other. Therefore, at the time when the Big Bang gave birth to the Universe, matter and anti-matter would have to be formed in equal amounts. But in this case they had to immediately annihilate. Since this did not happen, there had to be a mechanism to separate matter and anti-matter. The origin of this paradox or "baryonic asymmetry" is unclear. A solution to the paradox could be possible chirality of moving charged elementary particles. An interesting idea in favor of the existence of chirality of all moving charged elementary particles was proposed by Davankov [248,249]. He assumed that a moving electron (in metal wire or in vacuum) is accompanied by the appearance of a circular magnetic field of one particular direction. Thus, a system consisting of a moving electron and the resulting circular magnetic field is a chiral system. This idea leads to a conclusion that every charged elementary particle is inherently chiral. According to this idea, particles of the opposite charge (e.g., an electron and a positron) have opposite chirality (as enantiomers). Since each elementary particle has a symmetric pair—an anti-particle with the opposite charge, their chirality may be of a different sign. That is, they had an object-and-mirror image relation during the Big Bang.

A possible explanation of the paradox of "baryonic asymmetry" may be based on the assumption that in the Big Band there was a separation of material and anti-material particles as "enantiomers" (according Davankov's idea [248,249]). In accordance with Kozyrev's [250–254] concept of mirror reflection, they should diverge in the opposite time.

Kozyrev observed small difference in the weight of a spinning gyroscope clockwise and counterclockwise. Kozyrev suggested that the dependence of the gyroscope weight on the direction of rotation may be due to a violation of the casual relationship with respect to some external standard. Such a standard may be the physical field of time. He argued the concept that time is energy that can concentrate, contract or stretch in small degree (maximum with coefficient 0.5). Kozyrev also established that time is reflected (as a flow of energy) by a mirror or smooth metal or stone surface. This hypothesis has been discussed and has its supporters [250–254].

Let's say that enantiomers being a mirror image of each other differ in the physical effects of time ("flow of time"). This difference is expressed in a change in the properties of the racemic mixture compared to enantiomers. However, the racemate and enantiomer remain in the "flow of time" of our Universe. In the absence of this flow (at the Big Bang) opposite material and anti-material enantiomers will be at different times after Big Bang. This idea explains the mystery of "baryon asymmetry".

A good confirmation of the aforementioned Kozyrev's experiment is the Dzhanibekov effect or tennis racket theorem. (Chapter 7). Indeed, a spherical object rotating in space can be considered as two hemispheres connected by bottoms. One hemisphere, which is set upward by the pole, rotates clockwise, another hemisphere setting upward by pole rotates counterclockwise (Figure 23), similar to" top" and "bottom" of our Galaxy [43]. A change in the weight of the hemispheres can lead to a periodic somersault of a spherical object (Dzhanibekov's effect). A possible difference in hemispheres is also distinction in meteorological (Earth [255–258] in the corresponding seasons) and irradiation (Sun asymmetry [224–226]) conditions of the northern and southern hemispheres.
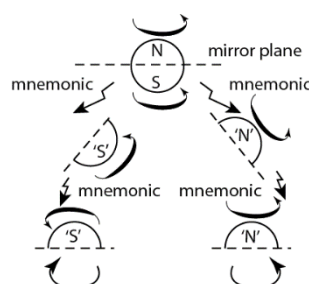

Figure 23. Schematic image of spin rotating Earth as two gyroscopes which bound by the bases.

Long ago it was noticed by sailors that crossing the equator changes the direction of the screw-sense of whirlpool of flowing water in the sink. This observation also supports the consideration of the equator as the plane of mirror symmetry (or the function associated with it) of a rotating spherical object as the globe.

According the abovementioned idea, our Universe is racemic mixture of matter and anti-matter (may be as "dark matter") universes. The annihilation of matter and anti-matter does not occur since both universes are in different times.

12. Conclusions

We endeavored to discuss all known facts concerning mirror symmetry and mirror reflection effects in chemistry and physics. The interpretation and analysis of these facts is based mainly on chemical thinking. However, we also proposed the analysis of these facts made by a physicist. Therefore, the joint interpretation of the facts is comprised of both molecular chemical and purely physical effects and theories:

1. An equal (50%:50%) mixture of molecules of a different chirality sign often changes physical properties both in crystal and in solution in comparison with pure enantiomers (Wallach's rule). The catalytic activity of metal complexes with racemic ligands also differs from the corresponding complexes with enantiomers (nonlinear effects). Moreover, there is an internal connection between Wallach's rule and nonlinear effects.

2. Helical polymers from achiral monomers form a mixture (50%:50%) of domains of molecules with a chirality sign which is different between the domains. This case resembles a conglomerate (mixture) of chiral crystals (Figure 1c) because a pool of helical molecules of one sign of chirality occupies the entire domain, while approximately the same area of the domain with chiral molecules of another sign occupies the adjacent area. Domains of molecules of different chirality signs are similar to crystals of the Pasteur's crystal mixture (conglomerate).

3. Helical chains of polymers of achiral molecules (including inorganic salts or ferromagnetic salts in magnetic fields) often contain helical fragments of inversed chirality.

4. Even structurally stable double helix of DNA reinforced with internal straps (nucleotide bases) comprise such sites (B–Z DNA transition). However, only triads of right-handed single, double and triple helices act properly in life processes, whereas the left-handed sites may cause damage (e.g., in the presence of sites with the B–Z DNA transition, the living organisms respond to it by genetic diseases).

5. The mirror symmetry effect is also inherent in other physical objects and phenomena (various moving objects, organs of living beings, water flows, material and anti-material particles, etc.).

Author Contributions: Conceptualization, V.A.P.; methodology, V.A.P.; validation, V.A.P.; writing—original draft preparation, V.A.P.; writing—review and editing, V.A.P.; writing—original draft preparation, Y.V.S.; visualization, Y.V.S.; supervision, Y.V.S.; supervision, S.G.Z.; funding acquisition, S.G.Z.; all authors have read and agreed to the published version of the manuscript.

References

1. Wallach, O. Zur Kenntniss der Terpene und der ätherischen Oele. *Justus Liebig's Ann. Chem.* **1895**, *286*, 90–118. [CrossRef]
2. Brock, C.P.; Schweizer, W.B.; Dunitz, J.D. On the validity of Wallach's rule: On the density and stability of racemic crystals compared with their chiral counterparts. *J. Am. Chem. Soc.* **1991**, *113*, 9811–9820. [CrossRef]
3. Ernst, K.-H. On the Validity of Calling Wallach's Rule Wallach's Rule. *Isr. J. Chem.* **2017**, *57*, 24–30. [CrossRef]
4. Bredikhin, A.A.; Lazarev, S.N.; Bredikhina, Z.A.; Savel, D.V.; Vandyukova, I.I.; Gubaidullin, A.T.; Litvinov, I.A. Crystallization of chiral compounds. 1. Spectroscopic, thermochemical, and crystallographic investigation of homochiral and racemic glycidyl p-toluenesulfonate. *Russ. Chem. Bull.* **2003**, *52*, 846–852. [CrossRef]

5. Slepukhin, P.A.; Gruzdev, D.A.; Chulakov, E.N.; Levit, G.L.; Krasnov, V.P.; Charushin, V.N. Structures of the racemate and (S)-enantiomer of 7,8-difluoro-3-methyl-2,3-dihydro-4H-[1,4]benzoxazine. *Russ. Chem. Bull.* **2011**, *60*, 955–960. [CrossRef]

6. Sakurai, T.; Masuda, Y.; Sato, H.; Yamagishi, A.; Kawaji, H.; Atake, T.; Hori, K. A Comparative Study on Chiral and Racemic 12-Hydroxyoctadecanoic Acids in the Solutions and Aggregation States: Does the Racemic Form Really Form a Gel? *Bull. Chem. Soc. Jpn.* **2010**, *83*, 145–150. [CrossRef]

7. Navare, P.S.; MacDonald, J.C. Investigation of Stability and Structure in Three Homochiral and Heterochiral Crystalline Forms of 3-Phenyllactic Acid. *Cryst. Growth Des.* **2011**, *11*, 2422–2428. [CrossRef]

8. Krishnaswamy, S.; Patil, M.T.; Shashidhar, M.S. Comparison of racemic epi-inosose and (-)-epi-inosose. *Acta Crystallogr. C* **2011**, *67*, o435–o438. [CrossRef]

9. Kitoh, S.-I.; Kunimoto, K.-K.; Funaki, N.; Senda, H.; Kuwae, A.; Hanai, K.J. Crystal structures and vibrational spectra of racemic and chiral 4-phenyl-1,3-oxazolidine-2-thione. *Chem. Crystallogr.* **2002**, *32*, 547–553. [CrossRef]

10. Friscic, T.; Fabian, L.; Burley, J.C.; Reid, D.G.; Duer, M.J.; Jones, W. Exploring the relationship between cocrystal stability and symmetry: Is Wallach's rule applicable to multi-component solids? *Chem. Commun.* **2008**, 1644–1646. [CrossRef]

11. Sørensen, H.O.; Larsen, S. Hydrogen bonding in enantiomericversusracemic mono-carboxylic acids; a case study of 2-phenoxypropionic acid. *Acta Crystallogr. B Struct. Sci.* **2003**, *59*, 132–140. [CrossRef] [PubMed]

12. Snyder, S.E.; Volkers, P.I.; Engebretson, D.A.; Lee, W.; Pirkle, W.H.; Carey, J.R. Strong enantioselective self-recognition of a small chiral molecule. *Org. Lett.* **2007**, *9*, 2341–2343. [CrossRef]

13. Jeong, K.S.; Kim, D.E.; Lee, E.; Jhon, Y.H.; Han, H.; Kim, J.; Jeong, N. Crystal structures of (2-substituted-5-N-tosyl)bicyclo[3.3.0]-5-azacyclooct-2-enone: A pseudo achiral crystal from enantiopure compound and a counter-example of Wallach's rule. *Tetrahedron Asymmetry* **2009**, *20*, 1736–1741. [CrossRef]

14. Cai, W.; He, J.; Li, W.; Katrusiak, A. Anomalous compression of a weakly CH···O bonded nonlinear optical molecular crystal. *J. Mater. Chem. C* **2014**, *2*, 6471–6476. [CrossRef]

15. Willer, R.L.; Storey, R.F.; Deschamps, J.; Parrish, D.; Kendrick, J.; Leusen, F.J.J. Synthesis, Prediction, and Determination of Crystal Structures of (R/S)- and (S)-1,6-Dinitro-3,8-dioxa-1,6-diazaspiro[4.4]nonane-2,7-dione. *Cryst. Growth Des.* **2012**, *12*, 5292–5297. [CrossRef]

16. Podsiadło, M.; Patyk, E.; Katrusiak, A. Chiral aggregation hierarchy in high-pressure resolved 2-butanol and 2,3-butanediol. *CrystEngComm* **2012**, *14*, 6419–6423. [CrossRef]

17. Khrustalev, V.N.; Sandhu, B.; Bentum, S.; Fonari, A.; Krivoshein, A.V.; Timofeeva, T.V. Absolute Configuration and Polymorphism of 2-Phenylbutyramide and alpha-Methyl-alpha-phenylsuccinimide. *Cryst. Growth Des.* **2014**, *14*, 3360–3369. [CrossRef]

18. Patrick, B.O.; Brock, C.P. S,S-1,2-Dicyclohexylethane-1,2-diol and its racemic compound: A striking exception to Wallach's rule. *Acta Crystallogr. B* **2006**, *62*, 488–497. [CrossRef]

19. Kennedy, A.R.; Morrison, C.A.; Briggs, N.E.B.; Arbuckle, W. Density and Stability Differences Between Enantiopure and Racemic Salts: Construction and Structural Analysis of a Systematic Series of Crystalline Salt Forms of Methylephedrine. *Cryst. Growth Des.* **2011**, *11*, 1821–1834. [CrossRef]

20. Cai, W.; Marciniak, J.; Andrzejewski, M.; Katrusiak, A. Pressure Effect on d,l-Mandelic Acid Racemate Crystallization. *J. Phys. Chem. C* **2013**, *117*, 7279–7285. [CrossRef]

21. Assaad, T.; Rukiah, M. Powder X-ray study of racemic (2RS,3RS)-5-amino-3-[4-(3-methoxyphenyl)piperazin-1-yl]-1,2,3,4-tetrahydronaphtha len-2-ol. *Acta Crystallogr. C* **2011**, *67*, o469–o472. [CrossRef] [PubMed]

22. Husin, H.; Leong, Y.-K.; Liu, J. Molecular attributes of an effective steric agent: Yield stress of dispersions in the presence of pure enantiomeric and racemate malic acids. *Adv. Powder Tech.* **2012**, *23*, 459–464. [CrossRef]

23. Sanabria, C.M.; Gomez, S.L.; Palma, A.; Cobo, J.; Glidewell, C. Four 1-naphthyl-substituted tetrahydro-1,4-epoxy-1-benzazepines: Hydrogen-bonded structures in one, two and three dimensions. *Acta Crystallogr. C* **2010**, *66*, o540–o546. [CrossRef]

24. Marthi, K.; Larsen, S.; Ács, M.; Fogassy, E. Enantiomer associations in the crystal structures of racemic and (2S,3S)-(+)-3-hydroxy-2-(4-methoxyphenyl)-2,3-dihydro-1,5-benzothiazepin-4(5H)-one. *J. Mol. Struct.* **1996**, *374*, 347–355. [CrossRef]

25. Luger, P.; Weber, M. DL-Cysteine at 298K. *Acta Crystallogr. C Cryst. Struct. Commun.* **1999**, *55*, 1882–1885. [CrossRef]

26. Pella, E.; Restelli, R. Binary phase diagram of the enantiomers of indoprofen. *Mikrochim. Acta* **1983**, *79*, 65–74. [CrossRef]

27. Xie, S.; Nusbaum, D.A.; Stein, H.J.; Pink, M. 4-(3-Methoxy-phen-yl)-2,6-dimethyl-cyclo-hex-3-enecarboxylic acid. *Acta Crystallogr. E Struct. Rep. Online* **2010**, *66*, o1443–o1449. [CrossRef]

28. Blazis, V.J.; Koeller, K.J.; Rath, N.P.; Spilling, C.D. Application of Wallach's Rule in a Comparison of the X-ray Crystal Structures of the Racemate and the (S) Enantiomer of (1-Hydroxy-3-phenyl-2-propenyl) Dimethylphosphonate. *Acta Crystallogr. B Struct. Sci.* **1997**, *53*, 838–842. [CrossRef]

29. Dunitz, J.D.; Gavezzotti, A. Proteogenic amino acids: Chiral and racemic crystal packings and stabilities. *J. Phys. Chem. B* **2012**, *116*, 6740–6750. [CrossRef]

30. Studniarz, S.A. The Solubility of Chiral Enantiomers and Racemates as a Function of Enthalpy Differences in the Crystalline solids and Activity Coefficients in the Solution. In Proceedings of the Abstracts 37th Middle Atlantic Regional Meeting of the American Chemical Society, New Brunswick, NJ, USA, 22–25 May 2005; p. GENE-543.

31. Tu, T.; Maris, T.; Wuest, J.D. Crystal Structures of Spiroborates Derived from [1,1'-Binaphthalene]-2,2'-diol (BINOL). *Cryst. Growth Des.* **2008**, *8*, 1541–1546. [CrossRef]

32. Wałejko, P.; Paradowska, K.; Szeleszczuk, Ł.; Wojtulewski, S.; Baj, A. Racemic crystals of trolox derivatives compared to their chiral counterparts: Structural studies using solid-state NMR, DFT calculations and X-ray diffraction. *J. Mol. Struct.* **2018**, *1156*, 290–300. [CrossRef]

33. Marciniak, J.; Andrzejewski, M.; Cai, W.; Katrusiak, A. Wallach's Rule Enforced by Pressure in Mandelic Acid. *J. Phys. Chem. C* **2014**, *118*, 4309–4313. [CrossRef]

34. Cai, W.; Katrusiak, A. Enantiomeric crystallization of (±)-trans-1,2-diaminocyclohexane under pressure. *CrystEngComm* **2011**, *13*, 6742–6746. [CrossRef]

35. Pidcock, E. Achiral molecules in non-centrosymmetric space groups. *Chem. Commun.* **2005**, 3457–3459. [CrossRef] [PubMed]

36. Pavlov, V.A.; Mistryukov, E.A.; Duddeck, H.; Vinogradov, M.G.; Snatzke, G. Stereochemistry in cross-coupling reaction of crotyl alcohol derivatives and arylmagnesium bromides on trans-bis-1S, 2S- and trans-bis-1R,2R-(diphenylphosphino) cyclopentanenickel dibromide. *J. Mol. Catal.* **1993**, *79*, 55–74. [CrossRef]

37. Kim, J.U.; Schollmeyer, D.; Brehmer, M.; Zentel, R. Simple chiral urea gelators, (R)- and (S)-2-heptylurea: Their gelling ability enhanced by chirality. *J. Colloid. Interface Sci.* **2011**, *357*, 428–433. [CrossRef] [PubMed]

38. Perlovich, G.L.; Kurkov, S.V.; Hansen, L.K.; Bauer-Brandl, A. Thermodynamics of sublimation, crystal lattice energies, and crystal structures of racemates and enantiomers: (+)- and (+/-)-ibuprofen. *J. Pharm. Sci.* **2004**, *93*, 654–666. [CrossRef] [PubMed]

39. Benson, N.; Snelder, N.; Ploeger, B.; Napier, C.; Sale, H.; Birdsall, N.J.; Butt, R.P.; van der Graaf, P.H. Estimation of binding rate constants using a simultaneous mixed-effects method: Application to monoamine transporter reuptake inhibitor reboxetine. *Br. J. Pharmacol.* **2010**, *160*, 389–398. [CrossRef]

40. Okuyama, K.; Morimoto, T.; Narita, H.; Kawaguchi, T.; Mizuno, K.; Bachinger, H.P.; Wu, G.; Noguchi, K. Two crystal modifications of (Pro-Pro-Gly)4-Hyp-Hyp-Gly-(Pro-Pro-Gly)4 reveal the puckering preference of Hyp(X) in the Hyp(X):Hyp(Y) and Hyp(X):Pro(Y) stacking pairs in collagen helices. *Acta Crystallogr. D Biol. Crystallogr.* **2010**, *66*, 88–96. [CrossRef]

41. Xu, F.; Khan, I.J.; McGuinness, K.; Parmar, A.S.; Silva, T.; Murthy, N.S.; Nanda, V. Self-assembly of left- and right-handed molecular screws. *J. Am. Chem. Soc.* **2013**, *135*, 18762–18765. [CrossRef]

42. Lin, S.Y.; Xu, G.F.; Zhao, L.; Guo, Y.N.; Guo, Y.; Tang, J. Observation of slow magnetic relaxation in triple-stranded lanthanide helicates. *Dalton Trans.* **2011**, *40*, 8213–8217. [CrossRef] [PubMed]

43. Pavlov, V.A.; Shushenachev, Y.V.; Zlotin, S.G. Chiral and Racemic Fields Concept for Understanding of the Homochirality Origin, Asymmetric Catalysis, Chiral Superstructure Formation from Achiral Molecules, and B-Z DNA Conformational Transition. *Symmetry* **2019**, *11*, 649. [CrossRef]

44. Le, K.V.; Takezoe, H.; Araoka, F. Chiral Superstructure Mesophases of Achiral Bent-Shaped Molecules—Hierarchical Chirality Amplification and Physical Properties. *Adv. Mater.* **2017**, *29*, 1602737. [CrossRef] [PubMed]

45. Otani, T.; Araoka, F.; Ishikawa, K.; Takezoe, H. Enhanced optical activity by achiral rod-like molecules nanosegregated in the B4 structure of achiral bent-core molecules. *J. Am. Chem. Soc.* **2009**, *131*, 12368–12372. [CrossRef]

46. Hough, L.E.; Spannuth, M.; Nakata, M.; Coleman, D.A.; Jones, C.D.; Dantlgraber, G.; Tschierske, C.; Watanabe, J.; Korblova, E.; Walba, D.M.; et al. Chiral isotropic liquids from achiral molecules. *Science* **2009**, *325*, 452–456. [CrossRef]

47. Takanishi, Y.; Shin, G.J.; Jung, J.C.; Choi, S.-W.; Ishikawa, K.; Watanabe, J.; Takezoe, H.; Toledano, P. Observation of very large chiral domains in a liquid crystal phase formed by mixtures of achiral bent-core and rod molecules. *J. Mater. Chem.* **2005**, *15*, 4020–4024. [CrossRef]

48. Kim, K.; Kim, H.; Jo, S.Y.; Araoka, F.; Yoon, D.K.; Choi, S.W. Photomodulated Supramolecular Chirality in Achiral Photoresponsive Rodlike Compounds Nanosegregated from the Helical Nanofilaments of Achiral Bent-Core Molecules. *ACS Appl. Mater. Interfaces* **2015**, *7*, 22686–22691. [CrossRef]

49. Nagayama, H.; Varshney, S.K.; Goto, M.; Araoka, F.; Ishikawa, K.; Prasad, V.; Takezoe, H. Spontaneous deracemization of disc-like molecules in the columnar phase. *Angew. Chem. Int. Ed. Engl.* **2010**, *49*, 445–448. [CrossRef]

50. Gortz, V.; Goodby, J.W. Enantioselective segregation in achiral nematic liquid crystals. *Chem. Commun.* **2005**, 3262–3264. [CrossRef]

51. Zhang, C.; Diorio, N.; Lavrentovich, O.D.; Jakli, A. Helical nanofilaments of bent-core liquid crystals with a second twist. *Nat. Commun.* **2014**, *5*, 3302. [CrossRef]

52. Hazen, R.M.; Sholl, D.S. Chiral selection on inorganic crystalline surfaces. *Nat. Mater.* **2003**, *2*, 367–374. [CrossRef]

53. Bonner, W.A.; Kavasmaneck, P.R.; Martin, F.S.; Flores, J.J. Asymmetric adsorption of alanine by quartz. *Science* **1974**, *186*, 143–144. [CrossRef] [PubMed]

54. Weissbuch, I.; Addadi, L.; Leiserowitz, L. Molecular recognition at crystal interfaces. *Science* **1991**, *253*, 637–645. [CrossRef]

55. Koretsky, C.M.; Sverjensky, D.A.; Sahai, N. A model of surface site types on oxide and silicate minerals based on crystal chemistry; implications for site types and densities, multi-site adsorption, surface infrared spectroscopy, and dissolution kinetics. *Am. J. Sci.* **1998**, *298*, 349–438. [CrossRef]

56. Dana, E.S. *A Text-book of Mineralogy: With an Extended Treatise on Crystallography and Physical Mineralogy*; John Wiley & Sons: New York, NY, USA, 1898. Available online: https://www.doc-developpement-durable. org/file/Mines-Mineurs/Livres/Dana-s%20textbook%20of%20Mineralogy.pdf (accessed on 28 May 2020).

57. Hazen, R.M.; Filley, T.R.; Goodfriend, G.A. Selective adsorption of L- and D-amino acids on calcite: Implications for biochemical homochirality. *Proc. Natl. Acad. Sci. USA* **2001**, *98*, 5487–5490. [CrossRef] [PubMed]

58. Van Cappellen, P.; Charlet, L.; Stumm, W.; Wersin, P. A surface complexation model of the carbonate mineral-aqueous solution interface. *Geochim. Cosmochim. Acta* **1993**, *57*, 3505–3518. [CrossRef]

59. Stipp, S.L.; Hochella, M.F. Structure and bonding environments at the calcite surface as observed with X-ray photoelectron spectroscopy (XPS) and low energy electron diffraction (LEED). *Geochim. Cosmochim. Acta* **1991**, *55*, 1723–1736. [CrossRef]

60. Bąbel, M. Crystal lography and genesis of the giant intergrowths of gypsum from the Miocene evaporites of Poland. *Arch. Miner.* **1990**, *44*, 103–135.

61. Cody, A.M.; Cody, R.D. Chiral habit modifications of gypsum from epitaxial-like adsorption of stereospecific growth inhibitors. *J. Cryst. Growth* **1991**, *113*, 508–519. [CrossRef]

62. Kondepudi, D.K.; Kaufman, R.J.; Singh, N. Chiral symmetry breaking in sodium chlorate crystallizaton. *Science* **1990**, *250*, 975–976. [CrossRef]

63. Kondepudi, D.K.; Laudadio, J.; Asakura, K. Chiral Symmetry Breaking in Stirred Crystallization of 1,1'-Binaphthyl Melt. *J. Am. Chem. Soc.* **1999**, *121*, 1448–1451. [CrossRef]

64. Asakura, K.; Soga, T.; Uchida, T.; Osanai, S.; Kondepudi, D.K. Probability distributions of enantiomeric excess in unstirred and stirred crystallization of 1,1'-binaphthyl melt. *Chirality* **2002**, *14*, 85–89. [CrossRef] [PubMed]

65. Viedma, C. Chiral symmetry breaking during crystallization: Complete chiral purity induced by nonlinear autocatalysis and recycling. *Phys. Rev. Lett.* **2005**, *94*, 065504. [CrossRef] [PubMed]

66. Pavlov, V.; Pavlova, T. Paradoxes of Symmetry: Homochirality; Cryptochiral Reactions; Chiral Field, Memory, and Induction; Chiral and Racemic Environment. *Curr. Org. Chem.* **2017**, *21*, 872–888. [CrossRef]

67. Pavlov, V.A.; Zlotin, S.G. Homochirality, Stochastic Chiral Reactions, Spontaneous Chiral Ordering of Achiral Molecules, and Similar Chiral Effects. Is there a Physical Basis for these Mirror Symmetry Breaking Phenomena?** *Curr. Org. Chem.* **2018**, *22*, 2029–2054. [CrossRef]

68. Han, B.; Shen, F.; Su, H.; Zhang, X.; Shen, Y.; Zhang, T. Self-assembly of achiral monomer into left-handed helical polyanthracene nanofibers. *Mater. Express* **2016**, *6*, 88–92. [CrossRef]

69. El-Hachemi, Z.; Arteaga, O.; Canillas, A.; Crusats, J.; Llorens, J.; Ribo, J.M. Chirality generated by flows in pseudocyanine dye J-aggregates: Revisiting 40 years old reports. *Chirality* **2011**, *23*, 585–592. [CrossRef]

70. Ribo, J.M.; Crusats, J.; Sagues, F.; Claret, J.; Rubires, R. Chiral sign induction by vortices during the formation of mesophases in stirred solutions. *Science* **2001**, *292*, 2063–2066. [CrossRef]

71. Micali, N.; Engelkamp, H.; van Rhee, P.G.; Christianen, P.C.; Monsu Scolaro, L.; Maan, J.C. Selection of supramolecular chirality by application of rotational and magnetic forces. *Nat. Chem.* **2012**, *4*, 201–207. [CrossRef]

72. Pavlov, V.A.; Spitsina, N.I.; Klabunovsky, E.I. Enantioselective hydrogenation in a cholesteric liquid crystal as a chiral matrix. *Bull. Acad. Sci. USSR Div. Chem. Sci.* **1982**, *31*, 2509. [CrossRef]

73. Pavlov, V.A.; Spitsina, N.I.; Klabunovsky, E.I. Enantioselective hydrogenation in cholesteryl tridecanoate as a chiral liquid-crystalline matrix. *Bull. Acad. Sci. USSR Div. Chem. Sci.* **1983**, *32*, 1501–1503. [CrossRef]

74. Ding, K.; Ishii, A.; Mikami, K. Super High Throuput Screening (SHTS) of Chiral Ligands and Activators: Asymmetric Activation of Chiral Diol-Zinc Catalysts by Chiral Nitrogen Activators for the Enantioselective Addition of Diethylzinc to Aldehydes. *Angew. Chem. Int. Ed.* **1999**, *38*, 497–501. [CrossRef]

75. Vyskočil, Š.; Jaracz, S.; Smrcina, M.; Štícha, M.; Hanuš, V.; Polášek, M.; Kočovský, P. Synthesis of N-Alkylated and N-Arylated Derivatives of 2-Amino-2′-hydroxy-1,1′-binaphthyl (NOBIN) and 2,2′-Diamino-1,1′-binaphthyl and Their Application in the Enantioselective Addition of Diethylzinc to Aromatic Aldehydes†. *J. Org. Chem.* **1998**, *63*, 7727–7737. [CrossRef]

76. Le Goanvic, D.; Holler, M.; Pale, P. Chiral tridentate versus bidentate pyridines as catalysts in the enantioselective alkylation of benzaldehyde with diethylzinc. *Tetrahedron: Asymmetry* **2002**, *13*, 119–121. [CrossRef]

77. Rosner, T.; Sears, P.J.; Nugent, W.A.; Blackmond, D.G. Kinetic Investigations of Product Inhibition in the Amino Alcohol-Catalyzed Asymmetric Alkylation of Benzaldehyde with Diethylzinc. *Org. Lett.* **2000**, *2*, 2511–2513. [CrossRef]

78. Satyanarayana, T.; Abraham, S.; Kagan, H.B. Nonlinear effects in asymmetric catalysis. *Angew. Chem. Int. Ed. Engl.* **2009**, *48*, 456–494. [CrossRef] [PubMed]

79. Puchot, C.; Samuel, O.; Dunach, E.; Zhao, S.; Agami, C.; Kagan, H.B. Nonlinear effects in asymmetric synthesis. Examples in asymmetric oxidations and aldolization reactions. *J. Am. Chem. Soc.* **1986**, *108*, 2353–2357. [CrossRef]

80. Guillaneux, D.; Zhao, S.-H.; Samuel, O.; Rainford, D.; Kagan, H.B. Nonlinear Effects in Asymmetric Catalysis. *J. Am. Chem. Soc.* **1994**, *116*, 9430–9439. [CrossRef]

81. Kitamura, M.; Okada, S.; Suga, S.; Noyori, R. Enantioselective addition of dialkylzincs to aldehydes promoted by chiral amino alcohols. Mechanism and nonlinear effect. *J. Am. Chem. Soc.* **1989**, *111*, 4028–4036. [CrossRef]

82. Noyori, R.; Kitamura, M. Enantioselective Addition of Organometallic Reagents to Carbonyl Compounds: Chirality Transfer, Multiplication, and Amplification. *Angew. Chem. Int. Ed. Eng.* **1991**, *30*, 49–69. [CrossRef]

83. Noyori, R.; Suga, S.; Oka, H.; Kitamura, M. Self and nonself recognition of chiral catalysts: The origin of nonlinear effects in the amino-alcohol catalyzed asymmetric addition of diorganozincs to aldehydes. *Chem. Rec.* **2001**, *1*, 85–100. [CrossRef] [PubMed]

84. Ercolani, G. Principles for designing an achiral receptor promoting asymmetric autocatalysis with amplification of chirality. *Tetrahedron Asymmetry* **2014**, *25*, 405–410. [CrossRef]

85. Tsukamoto, M.; Gopalaiah, K.; Kagan, H.B. Equilibrium of homochiral oligomerization of a mixture of enantiomers. Its relevance to nonlinear effects in asymmetric catalysis. *J. Phys. Chem. B* **2008**, *112*, 15361–15368. [CrossRef] [PubMed]

86. Balsells, J.; Costa, A.M.; Walsh, P.J. Temperature-dependent nonlinear effects and catalyst evolution in the asymmetric addition of diethylzinc to benzaldehyde. *Israel J. Chem.* **2001**, *41*, 251–262. [CrossRef]

87. Steigelmann, M.; Nisar, Y.; Rominger, F.; Goldfuss, B. Homo- and Heterochiral Alkylzinc Fencholates: Linear or Nonlinear Effects in Dialkylzinc Additions to Benzaldehyde. *Chem. Eur. J.* **2002**, *8*, 5211–5218. [CrossRef]

88. Chen, Y.K.; Costa, A.M.; Walsh, P.J. Substrate Dependence of Nonlinear Effects: Mechanistic Probe and Practical Applications. *J. Am. Chem. Soc.* **2001**, *123*, 5378–5379. [CrossRef]

89. Zarotti, P.; Knöpfel, T.F.; Aschwanden, P.; Carreira, E.M. Nonlinear Effects with Diastereomeric Ligand Mixtures in Enantioselective, Catalytic Additions of Terminal Alkynes Involving Copper–PINAP Complexes. *ACS Catal.* **2012**, *2*, 1232–1234. [CrossRef]

90. Demir, A.S.; Eymur, S. Nonlinear effects in proline–thiourea host–guest complex catalyzed aldol reactions in nonpolar solvents. *Tetrahedron Asymmetry* **2010**, *21*, 405–409. [CrossRef]

91. Soai, K.; Shibata, T.; Morioka, H.; Choji, K. Asymmetric autocatalysis and amplification of enantiomeric excess of a chiral molecule. *Nature* **1995**, *378*, 767–768. [CrossRef]

92. Soai, K.; Shibata, T.; Sato, I. Enantioselective automultiplication of chiral molecules by asymmetric autocatalysis. *Acc. Chem. Res.* **2000**, *33*, 382–390. [CrossRef]

93. Soai, K.; Kawasaki, T. Discovery of asymmetric autocatalysis with amplification of chirality and its implication in chiral homogeneity of biomolecules. *Chirality* **2006**, *18*, 469–478. [CrossRef] [PubMed]

94. Soai, K.; Soai, K.; Kawasaki, T. (S)-Diphenyl(1-methylpyrrolidin-2-yl)methanol. In Encycl. of Reag. for Org. Synthesis; John Wiley & Sons, Ltd.Hoboken, NJ, USA. pp. 1–33. [CrossRef]

95. Kawasaki, T.; Uchida, M.; Kaimori, Y.; Sasagawa, T.; Matsumoto, A.; Soai, K. Enantioselective Synthesis Induced by the Helical Molecular Arrangement in the Chiral Crystal of Achiral Tris(2-hydroxyethyl) 1,3,5-Benzenetricarboxylate in Conjunction with Asymmetric Autocatalysis. *Chem. Lett.* **2013**, *42*, 711–713. [CrossRef]

96. Schiaffino, L.; Ercolani, G. Amplification of chirality and enantioselectivity in the asymmetric autocatalytic Soai reaction. *ChemPhysChem* **2009**, *10*, 2508–2515. [CrossRef] [PubMed]

97. Sato, I.; Urabe, H.; Ishiguro, S.; Shibata, T.; Soai, K. Amplification of chirality from extremely low to greater than 99.5 % ee by asymmetric autocatalysis. *Angew. Chem. Int. Ed. Engl.* **2003**, *42*, 315–317. [CrossRef]

98. Bryliakov, K.P. Dynamic Nonlinear Effects in Asymmetric Catalysis. *ACS Catalysis* **2019**, *9*, 5418–5438. [CrossRef]

99. Pavlov, V.A. C_2 and C_1 Symmetry of chiral auxiliaries in catalytic reactions on metal complexes. *Tetrahedron* **2008**, *64*, 1147–1179. [CrossRef]

100. Pavlov, V.A.; Pavlova, T.N. Asymmetric metal complex catalysis in the series of monofunctional substrates: The lower the catalyst symmetry, the higher the enantioselectivity. *Russ. Chem. Rev.* **2010**, *79*, 881–905. [CrossRef]

101. Pavlov, V.A.; Pavlova, T.N. Influence of the Cn Symmetry of Chiral Catalyst on the Enantioselectivity of Reactions. *Curr. Org. Chem.* **2012**, *16*, 305–321. [CrossRef]

102. Pavlov, V.A.; Pavlova, T.N. Asymmetric induction in reactions catalyzed by metal complexes. *Russ. Chem. Rev.* **2012**, *81*, 823–854. [CrossRef]

103. Pavlov, V.A. Mechanisms of asymmetric induction in catalytic hydrogenation, hydrosilylation and cross-coupling on metal complexes. *Russ. Chem. Rev.* **2002**, *71*, 33–48. [CrossRef]

104. Pavlov, V.A. Structural and configurational relationships 'metal complex–substrate–product' in asymmetric catalytic hydrogenation, hydrosilylation and cross-coupling reactions. *Russ. Chem. Rev.* **2001**, *70*, 1037–1065. [CrossRef]

105. Thomson, R.J.; Jackson, W.R.; Haarburger, D.; Klabunovsky, E.I.; Pavlov, V.A. The Stereochemistry of Organometallic Compounds. XXIX. Synthesis of Steroidal 1,4-Diphosphine, 1,3-Diphosphine and 1,6-Diphosphine and Their Evaluation as Ligands in Metal Catalyzed Asymmetric Synthesis. *Aust. J. Chem.* **1987**, *40*, 1083–1106. [CrossRef]

106. Kiabutnovskii, B.I.; Vedenyapin, A.A.; Karpeiskaya, E.I.; Pavlov, V.A. Enantioselective Hydrogenation on Dissymmetric Cu-Ni and Pd- Catalysts. In *Studies in Surface Science and Catalysis*; Seivama, T., Tanabe, K., Eds.; Elsevier: Amsterdam, The Netherlands, 1981; Volume 7, pp. 390–401. [CrossRef]

107. Brown, M.K.; Blewett, M.M.; Colombe, J.R.; Corey, E.J. Mechanism of the enantioselective oxidation of racemic secondary alcohols catalyzed by chiral Mn(III)-salen complexes. *J. Am. Chem. Soc.* **2010**, *132*, 11165–11170. [CrossRef]

108. Petit-Garrido, N.; Ignes-Mullol, J.; Claret, J.; Sagues, F. Chiral selection by interfacial shearing of self-assembled achiral molecules. *Phys. Rev. Lett.* **2009**, *103*, 237802. [CrossRef] [PubMed]

109. Berg, A.M.; Patrick, D.L. Preparation of chiral surfaces from achiral molecules by controlled symmetry breaking. *Angew. Chem. Int. Ed. Engl.* **2005**, *44*, 1821–1823. [CrossRef]

110. Cai, Y.; Bernasek, S.L. Adsorption-induced asymmetric assembly from an achiral adsorbate. *J. Am. Chem. Soc.* **2004**, *126*, 14234–14238. [CrossRef]

111. Karakalos, S.; Zaera, F. Amplification of Enantioselectivity on Solid Surfaces Using Nonchiral Adsorbates. *J. Phys. Chem. C* **2015**, *119*, 13785–13790. [CrossRef]

112. Izumi, Y. Modified Raney Nickel (MRNi) Catalyst: Heterogeneous Enantio-Differentiating (Asymmetric) Catalyst. In *Advances in Catalysis*; Eley, D.D., Pines, H., Weisz, P.B., Eds.; Academic Press: New York, NY, USA, 1983; Volume 32, pp. 215–271.

113. Tai, A.; Harada, T. *Tailored Metal Catalysts*; Iwasawa, Y., Ed.; Reidel: Dordrecht, The Netherlands, 1986.

114. Krylov, O.V. *Heterogeneous Catalysis*; Akademkniga: Moscow, Russia, 2004; p. 679. (In Russian)

115. Raval, R. Chiral expression from molecular assemblies at metal surfaces: Insights from surface science techniques. *Chem. Soc. Rev.* **2009**, *38*, 707–721. [CrossRef]

116. Linares, M.; Minoia, A.; Brocorens, P.; Beljonne, D.; Lazzaroni, R. Expression of chirality in molecular layers at surfaces: Insights from modelling. *Chem. Soc. Rev.* **2009**, *38*, 806–816. [CrossRef]

117. Elemans, J.A.; De Cat, I.; Xu, H.; De Feyter, S. Two-dimensional chirality at liquid-solid interfaces. *Chem. Soc. Rev.* **2009**, *38*, 722–736. [CrossRef]

118. Ernst, K.H. Surface chemistry: Single handedness in flatland. *Nat. Chem.* **2017**, *9*, 195–196. [CrossRef] [PubMed]

119. Ernst, K.-H. Supramolecular Surface Chirality. In *Supramolecular Chirality*; Crego-Calama, M., Reinhoudt, D.N., Eds.; Springer: Berlin/Heidelberg, Germany, 2006; pp. 209–252. [CrossRef]

120. Barlow, S.M.; Raval, R. Complex organic molecules at metal surfaces: Bonding, organisation and chirality. *Surf. Sci. Rep.* **2003**, *50*, 201–341. [CrossRef]

121. Humblot, V.; Lorenzo, M.O.; Baddeley, C.J.; Haq, S.; Raval, R. Local and global chirality at surfaces: Succinic acid versus tartaric acid on Cu110. *J. Am. Chem. Soc.* **2004**, *126*, 6460–6469. [CrossRef] [PubMed]

122. Forster, M.; Dyer, M.S.; Persson, M.; Raval, R. Tailoring homochirality at surfaces: Going beyond molecular handedness. *J. Am. Chem. Soc.* **2011**, *133*, 15992–16000. [CrossRef] [PubMed]

123. Zaera, F. Chiral Modification of Solid Surfaces: A Molecular View. *J. Phys. Chem. C* **2008**, *112*, 16196–16203. [CrossRef]

124. Lorenzo, M.O.; Haq, S.; Bertrams, T.; Murray, P.; Raval, R.; Baddeley, C.J. Creating Chiral Surfaces for Enantioselective Heterogeneous Catalysis: R,R-Tartaric Acid on Cu(110). *J. Phys. Chem. B* **1999**, *103*, 10661–10669. [CrossRef]

125. Amharar, Y.; Petit, S.; Sanselme, M.; Cartigny, Y.; Petit, M.-N.l.; Coquerel, G.r. Crystal Structures, Dehydration Mechanism, and Chiral Discrimination in the Solid State of a Hydantoin Derivative. *Cryst. Growth Des.* **2011**, *11*, 2453–2462. [CrossRef]

126. Singh, G.; Chan, H.; Baskin, A.; Gelman, E.; Repnin, N.; Kral, P.; Klajn, R. Self-assembly of magnetite nanocubes into helical superstructures. *Science* **2014**, *345*, 1149–1153. [CrossRef]

127. Curie, P. Sur la symétrie dans les phénomènes physiques, symétrie d'un champ électrique et d'un champ magnétique. *J. Phys. Theor. Appl.* **1894**, *3*, 393–415. [CrossRef]

128. Klabunovski, J.I. *L'origine de la vie. Quelques aspects du probleme*; Gauthier-Villars: Paris, France, 1962; pp. 152–162.

129. Green, M.M.; Peterson, N.C.; Sato, T.; Teramoto, A.; Cook, R.; Lifson, S. A helical polymer with a cooperative response to chiral information. *Science* **1995**, *268*, 1860–1866. [CrossRef]

130. Lifson, S.; Felder, C.E.; Green, M.M. Helical conformations, internal motion, and helix sense reversal in polyisocyanates and the preferred helix sense of an optically active polyisocyanate. *Macromolecules* **1992**, *25*, 4142–4148. [CrossRef]

131. Celik-Aktas, A.; Zuo, J.M.; Stubbins, J.F.; Tang, C.; Bando, Y. Double-helix structure in multiwall boron nitride nanotubes. *Acta Crystallogr. A* **2005**, *61*, 533–541. [CrossRef] [PubMed]

132. Zhi, C.; Bando, Y.; Tang, C.; Golberg, D. Boron nitride nanotubes. *Mater. Sci. Eng. R* **2010**, *70*, 92–111. [CrossRef]

133. Ma, R.; Bando, Y.; Sato, T. Controlled Synthesis of BN Nanotubes, Nanobamboos, and Nanocables. *Adv. Mater.* **2002**, *14*. [CrossRef]

134. Zhigang Wang, D. A helix theory for molecular chirality and chiral interaction. *Mendeleev Commun.* **2004**, *14*, 244–247. [CrossRef]

135. Wang, D.Z. Conservation of helical asymmetry in chiral interactions. *Tetrahedron* **2005**, *61*, 7125–7133. [CrossRef]

136. Wang, D.Z. Catalyst–substrate helical character matching determines enantiomeric excess. *Tetrahedron* **2005**, *61*, 7134–7143. [CrossRef]

137. Wang, D.Z. Conservation of helicity and helical character matching in chiral interactions. *Chirality* **2005**, *17*, S177–S182. [CrossRef]

138. Giri, S.; Wang, D.Z.; Chattaraj, P.K. Catalyst electronic polarizability and enantiomeric excess in asymmetric hydrogenation. *Tetrahedron* **2010**, *66*, 4560–4563. [CrossRef]

139. Rouhi, A.M. Conservation of Helical Asymmetry. *Chem. Eng. News Arch.* **2003**, *81*, 34–35. [CrossRef]

140. Han, P.; Wang, R.; Wang, D.Z. Electronic polarizability-based stereochemical model for Sharpless AD reactions. *Tetrahedron* **2011**, *67*, 8873–8878. [CrossRef]

141. Wells, R.D. Non-B DNA conformations, mutagenesis and disease. *Trends Biochem. Sci.* **2007**, *32*, 271–278. [CrossRef]

142. Wells, R.D.; Dere, R.; Hebert, M.L.; Napierala, M.; Son, L.S. Advances in mechanisms of genetic instability related to hereditary neurological diseases. *Nucleic Acids. Res.* **2005**, *33*, 3785–3798. [CrossRef]

143. Zhang, H.; Yu, H.; Ren, J.; Qu, X. Reversible B/Z-DNA transition under the low salt condition and non-B-form polydApolydT selectivity by a cubane-like europium-L-aspartic acid complex. *Biophys. J.* **2006**, *90*, 3203–3207. [CrossRef] [PubMed]

144. Mirkin, S.M. DNA structures, repeat expansions and human hereditary disorders. *Curr. Opin. Struct. Biol.* **2006**, *16*, 351–358. [CrossRef] [PubMed]

145. Bacolla, A.; Wells, R.D. Non-B DNA conformations, genomic rearrangements, and human disease. *J. Biol. Chem.* **2004**, *279*, 47411–47414. [CrossRef] [PubMed]

146. Lupski, J.R. Genomic disorders: Structural features of the genome can lead to DNA rearrangements and human disease traits. *Trends Genet.* **1998**, *14*, 417–422. [CrossRef]

147. Lupski, J.R.; Stankiewicz, P. *Genomic Disorders: The Genomic BAsis of Desease*; Humana Press: Berlin, Germany, 2006.

148. Wells, R.D.; Ashizawa, T. (Eds.) *Genetic Instabilities and Neurological Diseases*; Academic Press: Houston, TX, USA, 2006.

149. Harvey, S.C. DNA structural dynamics: Longitudinal breathing as a possible mechanism for the B ⇆ Z transition. *Nucleic Acids Res.* **1983**, *11*, 4867–4878. [CrossRef]

150. Ha, S.C.; Lowenhaupt, K.; Rich, A.; Kim, Y.G.; Kim, K.K. Crystal structure of a junction between B-DNA and Z-DNA reveals two extruded bases. *Nature* **2005**, *437*, 1183–1186. [CrossRef]

151. Kim, D.; Reddy, S.; Kim, D.Y.; Rich, A.; Lee, S.; Kim, K.K.; Kim, Y.G. Base extrusion is found at helical junctions between right- and left-handed forms of DNA and RNA. *Nucleic Acids Res.* **2009**, *37*, 4353–4359. [CrossRef] [PubMed]

152. Kim, D.; Hur, J.; Han, J.H.; Ha, S.C.; Shin, D.; Lee, S.; Park, S.; Sugiyama, H.; Kim, K.K. Sequence preference and structural heterogeneity of BZ junctions. *Nucleic Acids Res.* **2018**, *46*, 10504–10513. [CrossRef] [PubMed]

153. Subramani, V.K.; Ravichandran, S.; Bansal, V.; Kim, K.K. Chemical-induced formation of BZ-junction with base extrusion. *Biochem. Biophys. Res. Commun.* **2019**, *508*, 1215–1220. [CrossRef] [PubMed]

154. Hopkins, R.C. Transitions between B-DNA and Z-DNA: A dilemma. *J. Theor. Biol.* **1983**, *101*, 327–333. [CrossRef]

155. Bothe, J.R.; Lowenhaupt, K.; Al-Hashimi, H.M. Sequence-specific B-DNA flexibility modulates Z-DNA formation. *J. Am. Chem. Soc.* **2011**, *133*, 2016–2018. [CrossRef]

156. Li, H.; Xiao, J.; Li, J.; Lu, L.; Feng, S.; Droge, P. Human genomic Z-DNA segments probed by the Z alpha domain of ADAR1. *Nucleic Acids Res.* **2009**, *37*, 2737–2746. [CrossRef] [PubMed]

157. Lee, J.; Kim, Y.G.; Kim, K.K.; Seok, C. Transition between B-DNA and Z-DNA: Free energy landscape for the B-Z junction propagation. *J. Phys. Chem. B* **2010**, *114*, 9872–9881. [CrossRef]

158. Premilat, S.; Albiser, G. Helix-helix transitions in DNA: Fibre X-ray study of the particular cases poly(dG-dC). poly(dG-dC) and poly(dA). 2poly(dT). *Eur. Biophys. J.* **1999**, *28*, 574–582. [CrossRef]

159. Pohl, F.M.; Jovin, T.M. Salt-induced co-operative conformational change of a synthetic DNA: Equilibrium and kinetic studies with poly(dG-dC). *J. Mol. Biol.* **1972**, *67*, 375–396. [CrossRef]

160. Zacharias, W.; Martin, J.C.; Wells, R.D. A condensed form of (dG-dC)$_n$.cntdot.(dG-dC)$_n$ as an intermediate between the B- and Z- conformations induced by sodium acetate. *Biochemistry* **2002**, *22*, 2398–2405. [CrossRef]

161. Wang, A.J.; Quigley, G.J.; Kolpak, F.J.; van der Marel, G.; van Boom, J.H.; Rich, A. Left-handed double helical DNA: Variations in the backbone conformation. *Science* **1981**, *211*, 171–176. [CrossRef] [PubMed]

162. Wang, A.H.; Quigley, G.J.; Kolpak, F.J.; Crawford, J.L.; van Boom, J.H.; van der Marel, G.; Rich, A. Molecular structure of a left-handed double helical DNA fragment at atomic resolution. *Nature* **1979**, *282*, 680–686. [CrossRef] [PubMed]

163. Behe, M.; Felsenfeld, G. Effects of methylation on a synthetic polynucleotide: The B–Z transition in poly(dG-m5dC).poly(dG-m5dC). *Proc. Natl. Acad. Sci. USA* **1981**, *78*, 1619–1623. [CrossRef] [PubMed]

164. Russell, W.C.; Precious, B.; Martin, S.R.; Bayley, P.M. Differential promotion and suppression of Z leads to B transitions in poly[d(G-C)] by histone subclasses, polyamino acids and polyamines. *EMBO J.* **1983**, *2*, 1647–1653. [CrossRef] [PubMed]

165. Pohl, F.M. Polymorphism of a synthetic DNA in solution. *Nature* **1976**, *260*, 365–366. [CrossRef]

166. Feigon, J.; Wang, A.H.; van der Marel, G.A.; Van Boom, J.H.; Rich, A. A one- and two-dimensional NMR study of the B to Z transition of (m5dC-dG)3 in methanolic solution. *Nucleic Acids Res.* **1984**, *12*, 1243–1263. [CrossRef]

167. Zimmer, C.; Tymen, S.; Marck, C.; Guschlbauer, W. Conformational transitions of poly(dA-dC).poly(dG-dT) induced by high salt or in ethanolic solution. *Nucleic Acids Res.* **1982**, *10*, 1081–1091. [CrossRef]

168. van de Sande, J.H.; McIntosh, L.P.; Jovin, T.M. Mn2+ and other transition metals at low concentration induce the right-to-left helical transformation of poly[d(G-C)]. *EMBO J.* **1982**, *1*, 777–782. [CrossRef]

169. Pohl, F.M.; Jovin, T.M.; Baehr, W.; Holbrook, J.J. Ethidium Bromide as a Cooperative Effector of a DNA Structure. *Proc. Natl. Acad. Sci. USA* **1972**, *69*, 3805–3809. [CrossRef]

170. Mirau, P.A.; Kearns, D.R. The effect of Intercalating drugs on the kinetics of the B to Z transition of poly(dG–dC). *Nucleic Acids Res.* **1983**, *11*, 1931–1941. [CrossRef]

171. Zacharias, W.; Larson, J.E.; Klysik, J.; Stirdivant, S.M.; Wells, R.D. Conditions which cause the right-handed to left-handed DNA conformational transitions. Evidence for several types of left-handed DNA structures in solution. *J. Biol. Chem.* **1982**, *257*, 2775–2782.

172. Wu, Z.; Tian, T.; Yu, J.; Weng, X.; Liu, Y.; Zhou, X. Formation of sequence-independent Z-DNA induced by a ruthenium complex at low salt concentrations. *Angew. Chem. Int. Ed. Engl.* **2011**, *50*, 11962–11967. [CrossRef] [PubMed]

173. Johnson, A.; Qu, Y.; Van Houten, B.; Farrell, N. B↑Z DNA conformational changes induced by a family of dinuclear bis(platinum) complexes. *Nucleic Acids Res.* **1992**, *20*, 1697–1703. [CrossRef] [PubMed]

174. Xu, Y.; Zhang, Y.X.; Sugiyama, H.; Umano, T.; Osuga, H.; Tanaka, K. (P)-helicene displays chiral selection in binding to Z-DNA. *J. Am. Chem. Soc.* **2004**, *126*, 6566–6567. [CrossRef] [PubMed]

175. Boulikas, T. Evolutionary consequences of nonrandom damage and repair of chromatin domains. *J. Mol. Evol.* **1992**, *35*, 156–180. [CrossRef]

176. Scarfí, M.R.; Sannino, A.; Perrotta, A.; Sarti, M.; Mesirca, P.; Bersani, F. Evaluation of Genotoxic Effects in Human Fibroblasts after Intermittent Exposure to 50 Hz Electromagnetic Fields: A Confirmatory Study. *Radiat. Res.* **2005**, *164*, 270–276. [CrossRef]

177. Lopez-Diaz, B.; Mercado-Saenz, S.; Martinez-Morillo, M.; Sendra-Portero, F.; Ruiz-Gomez, M.J. Long-term exposure to a pulsed magnetic field (1.5 mT, 25 Hz) increases genomic DNA spontaneous degradation. *Electromagn. Biol. Med.* **2014**, *33*, 228–235. [CrossRef]

178. Kim, J.; Ha, C.S.; Lee, H.J.; Song, K. Repetitive exposure to a 60-Hz time-varying magnetic field induces DNA double-strand breaks and apoptosis in human cells. *Biochem. Biophys. Res. Commun.* **2010**, *400*, 739–744. [CrossRef]

179. Ivancsits, S.; Diem, E.; Pilger, A.; Rüdiger, H.W.; Jahn, O. Induction of DNA strand breaks by intermittent exposure to extremely-low-frequency electromagnetic fields in human diploid fibroblasts. *Mutat. Res. Genet. Toxicol. Environ. Mutagen.* **2002**, *519*, 1–13. [CrossRef]

180. Wolf, F.I.; Torsello, A.; Tedesco, B.; Fasanella, S.; Boninsegna, A.; D'Ascenzo, M.; Grassi, C.; Azzena, G.B.; Cittadini, A. 50-Hz extremely low frequency electromagnetic fields enhance cell proliferation and DNA damage: Possible involvement of a redox mechanism. *Biochim. Biophys. Acta.* **2005**, *1743*, 120–129. [CrossRef]

181. Igarashi, A.; Kobayashi, K.; Matsuki, H.; Endo, G.; Haga, A. Evaluation of damage in DNA molecules resulting from very-low-frequency magnetic fields by using bacterial mutation repairing genetic system. *IEEE Trans. Magn.* **2005**, *41*, 4368–4370. [CrossRef]

182. Lai, H.; Singh, N.P. Magnetic-field-induced DNA strand breaks in brain cells of the rat. *Environ. Health Perspect.* **2004**, *112*, 687–694. [CrossRef] [PubMed]

183. Ruiz-Gómez, M.J.; Martínez-Morillo, M. Electromagnetic fields and the induction of DNA strand breaks. *Electromagn. Biol. Med.* **2009**, *28*, 201–214. [CrossRef] [PubMed]

184. McNamee, J.P.; Bellier, P.V.; Chauhan, V.; Gajda, G.B.; Lemay, E.; Thansandote, A. Evaluating DNA Damage in Rodent Brain after Acute 60 Hz Magnetic-Field Exposure. *Radiat. Res.* **2005**, *164*, 791–797. [CrossRef] [PubMed]

185. Li, S.H.; Chow, K.C. Magnetic field exposure induces DNA degradation. *Biochem. Biophys. Res. Commun.* **2001**, *280*, 1385–1388. [CrossRef] [PubMed]

186. Williams, P.A.; Ingebretsen, R.J.; Dawson, R.J. 14.6 mT ELF magnetic field exposure yields no DNA breaks in model system Salmonella, but provides evidence of heat stress protection. *Bioelectromagnetics* **2006**, *27*, 445–450. [CrossRef]

187. Kondepudi, D.K.; Asakura, K. Chiral Autocatalysis, Spontaneous Symmetry Breaking, and Stochastic Behavior. *Acc. Chem. Res.* **2001**, *34*, 946–954. [CrossRef]

188. Kondepudi, D.K.; Bullock, K.L.; Digits, J.A.; Hall, J.K.; Miller, J.M. Kinetics of chiral symmetry breaking in crystallization. *J. Am. Chem. Soc.* **1993**, *115*, 10211–10216. [CrossRef]

189. McBride, J.M.; Carter, R.L. Spontaneous Resolution by Stirred Crystallization. *Angew. Chem. Int. Ed. Engl.* **1991**, *30*, 293–295. [CrossRef]

190. Tomsett, M.; Maffucci, I.; Le Bailly, B.A.F.; Byrne, L.; Bijvoets, S.M.; Lizio, M.G.; Raftery, J.; Butts, C.P.; Webb, S.J.; Contini, A.; et al. A tendril perversion in a helical oligomer: Trapping and characterizing a mobile screw-sense reversal. *Chem. Sci.* **2017**, *8*, 3007–3018. [CrossRef]

191. Dzhanibekov effect or tennis racket theorem (Wolfram Community forum discussion about the Dzhanibekov Effect or tennis racket theorem). The effect was called after cosmonaut Vladimir Dzhanibecov who documented it in space, aboard the Soviet space station Salyut 7, in 1985. Available online: https://mathoverflow.net/questions/81960/the-dzhanibekov-effect-an-exercise-in-mechanics-or-ficition-explain-mathemat(accessed on 28 May 2020).

192. Bryson, B. *Short History of Nearly Everything*; Marsh Adency Ltd.: London, UK, 2003. Available online: https://www.goodreads.com/book/show/21.A_Short_History_of_Nearly_Everything (accessed on 28 May 2020).

193. Taxue, L.; Butler, R.; Banerjee, S.K.; van der Voo, R. *Essentials of Paleomagnetism*; University of California Press: Berkeley, CA, USA, 2009. Available online: https://earthref.org/MagIC/books/Tauxe/Essentials/ (accessed on 28 May 2020).

194. Pavlov, V.A.; Klabunovskii, E.I. The origin of homochirality in nature: A possible version. *Russ. Chem. Rev.* **2015**, *84*, 121–133. [CrossRef]

195. Pavlov, V.; Klabunovskii, E. Homochirality Origin in Nature: Possible Versions. *Curr. Org. Chem.* **2014**, *18*, 93–114. [CrossRef]

196. Breslow, R. Formation of L Amino Acids and D Sugars, and Amplification of their Enantioexcesses in Aqueous Solutions, Under Simulated Prebiotic Conditions. *Isr. J. Chem.* **2011**, *51*, 990–996. [CrossRef]

197. Weissbuch, I.; Lahav, M. Crystalline architectures as templates of relevance to the origins of homochirality. *Chem. Rev.* **2011**, *111*, 3236–3267. [CrossRef] [PubMed]

198. Lahav, M.; Weissbuch, I.; Shavit, E.; Reiner, C.; Nicholson, G.J.; Schurig, V. Parity violating energetic difference and enantiomorphous crystalsp-caveats; reinvestigation of tyrosine crystallization. *Orig. Life Evol. Biosph.* **2006**, *36*, 151–170. [CrossRef] [PubMed]

199. Meierhenrich, U.J. Amino Acids and the Asymmetry of Life. *Eur. Rev.* **2013**, *21*, 190–199. [CrossRef]

200. Evans, A.C.; Meinert, C.; Giri, C.; Goesmann, F.; Meierhenrich, U.J. Chirality, photochemistry and the detection of amino acids in interstellar ice analogues and comets. *Chem. Soc. Rev.* **2012**, *41*, 5447–5458. [CrossRef] [PubMed]

201. Lente, G. Open system approaches in deterministic models of the emergence of homochirality. *Chirality* **2010**, *22*, 907–913. [CrossRef]

202. Pizzarello, S. The chemistry of life's origin: A carbonaceous meteorite perspective. *Acc. Chem. Res.* **2006**, *39*, 231–237. [CrossRef]

203. Jorissen, A.; Cerf, C. Asymmetric Photoreactions as the Origin of Biomolecular Homochirality: A Critical Review. *Orig. Life Evol. Biosph.* **2002**, *32*, 129–142. [CrossRef]

204. Podlech, J. Origin of organic molecules and biomolecular homochirality. *Cell. Mol. Life Sci.* **2001**, *58*, 44–60. [CrossRef]

205. Carroll, J.D. A new definition of life. *Chirality* **2009**, *21*, 354–358. [CrossRef] [PubMed]

206. Barron, L.D. True and false chirality and absolute asymmetric synthesis. *J. Am. Chem. Soc.* **1986**, *108*, 5539–5542. [CrossRef]

207. He, Y.J.; Qi, F.; Qi, S.C. Earth's orbital chirality and driving force of biomolecular evolution. *Med. Hypotheses* **2001**, *56*, 493–496. [CrossRef] [PubMed]

208. He, Y.J.; Qi, F.; Qi, S.C. Periodicity of Earth's orbital chirality and possible mechanism of biological rhythms. *Med. Hypotheses* **2000**, *55*, 253–256. [CrossRef] [PubMed]

209. He, Y.J.; Qi, F.; Qi, S.C. Effect of earth's orbital chirality on elementary particles and unification of chiral asymmetries in life on different levels. *Med. Hypotheses* **2000**, *54*, 783–785. [CrossRef] [PubMed]

210. He, Y.J.; Ql, F.; Ql, S.C. Effect of chiral helical force field on molecular helical enantiomers and possible origin of biomolecular homochirality. *Med. Hypotheses* **1998**, *51*, 125–128. [CrossRef]

211. Stone, E.C.; Cummings, A.C.; McDonald, F.B.; Heikkila, B.C.; Lal, N.; Webber, W.R. Voyager 1 explores the termination shock region and the heliosheath beyond. *Science* **2005**, *309*, 2017–2020. [CrossRef] [PubMed]

212. Shu, F.H. *The Physical Universe: An Introduction to Astronomy*; University Science Books; Mill Valley, Calif: Sasalito, CA, USA, 1982. Available online: https://www.researchgate.net/publication/234289751_Book-Review_-_the_Physical_Universe_-_an_Introduction_to_Astronomy (accessed on 28 May 2020).

213. Maoz, D. *Astrophysics in a Nutshell*; Princeton University Press: Princeton, NJ, USA, 2007; p. 268.

214. Decker, R.B.; Krimigis, S.M.; Roelof, E.C.; Hill, M.E.; Armstrong, T.P.; Gloeckler, G.; Hamilton, D.C.; Lanzerotti, L.J. Voyager 1 in the foreshock, termination shock, and heliosheath. *Science* **2005**, *309*, 2020–2024. [CrossRef]

215. Vidal-Madjar, A.; Laurent, C.; Bruston, P.; Audouze, J. Is the solar system entering a nearby interstellar cloud. *Astrophys. J.* **1978**, *223*. [CrossRef]

216. Abbott, B.P.; Abbott, R.; Abbott, T.D.; Abernathy, M.R.; Acernese, F.; Ackley, K.; Adams, C.; Adams, T.; Addesso, P.; Adhikari, R.X.; et al. Observation of Gravitational Waves from a Binary Black Hole Merger. *Phys. Rev. Lett.* **2016**, *116*, 061102. [CrossRef]

217. Fischbach, E.; Buncher, J.B.; Gruenwald, J.T.; Jenkins, J.H.; Krause, D.E.; Mattes, J.J.; Newport, J.R. Time-Dependent Nuclear Decay Parameters: New Evidence for New Forces? *Space Sci. Rev.* **2009**, *145*, 285–335. [CrossRef]

218. Fischbach, E.; Chen, K.J.; Gold, R.E.; Goldsten, J.O.; Lawrence, D.J.; McNutt, R.J.; Rhodes, E.A.; Jenkins, J.H.; Longuski, J. Solar influence on nuclear decay rates: Constraints from the MESSENGER mission. *Astrophys. Space Sci.* **2011**, *337*, 39–45. [CrossRef]

219. Sturrock, P.A.; Buncher, J.B.; Fischbach, E.; Javorsek, D., II; Jenkins, J.H.; Mattes, J.J. Concerning the Phases of the Annual Variations of Nuclear Decay Rates. *Astrophys. J.* **2011**, 737. [CrossRef]

220. Silverman, M.P. Search for anomalies in the decay of radioactive Mn-54. *EPL Europhys. Lett.* **2016**, *114*, 62001. [CrossRef]

221. O'Keefe, D.; Morreale, B.L.; Lee, R.H.; Buncher, J.B.; Jenkins, J.H.; Fischbach, E.; Gruenwald, T.; Javorsek, D.; Sturrock, P.A. Spectral content of 22Na/44Ti decay data: Implications for a solar influence. *Astrophys. Space Sci.* **2013**, *344*, 297–303. [CrossRef]

222. Norman, E.B.; Browne, E.; Shugart, H.A.; Joshi, T.H.; Firestone, R.B. Evidence against correlations between nuclear decay rates and Earth–Sun distance. *Astroparticle Phys.* **2009**, *31*, 135–137. [CrossRef]

223. Norman, E.B.; Rech, G.A.; Browne, E.; Larimer, R.M.; Dragowsky, M.R.; Chan, Y.D.; Isaac, M.C.P.; McDonald, R.J.; Smith, A.R. Influence of physical and chemical environments on the decay rates of 7Be and 40K. *Phys. Lett. B* **2001**, *519*, 15–22. [CrossRef]

224. Ivanova, T.A.; Kuznettsov, S.N.; Logachev, Y.I.; Sosnovetc, E.N. North-south asymmetry and anisotropy of solar cosmic rays during the flare of April 18, 1972. *Kosmicheskie issledovaniya* **1976**, *14*, 235–238. (In Russian)

225. Svirzhevsky, N.S.; Svirzhevskaya, A.K.; Bazilevskaya, G.A.; Stozhkov, Y.I. North–South asymmetry in cosmic ray fluxes as measured in the stratosphere and in selected solar wind parameters in the near-Earth space. *Adv. Space Res.* **2005**, *35*, 671–676. [CrossRef]

226. El-Borie, M.A.; El-Abshehy, M.; Talaat, S.; Taleb, W.M.A. North-south asymmetry in solar, interplanetary, and geomagnetic indices. *Astrophysics* **2012**, *55*, 127–139. [CrossRef]

227. Tarasov, V.N. Sayana-Shushenskaya accident: Facts and hypotheses. *Sci. Life* **2013**, *7*, 18–30. (In Russian)

228. Kurzin, V.B.; Seleznev, V.S. Mechanism of emergence of intense vibrations of turbines on the Sayano-Shushensk hydro power plant. *J. Appl. Mech. Tech. Phys.* **2010**, *51*, 590–597. [CrossRef]

229. Lobanovsky Yu, I. Self-oscillations of pressure system and destruction of hydraulic units. *Hydraul. Eng.* **2010**, *7*, 39–45. Available online: http://www.plotina.net/experts/lobanovsky-2010/ (accessed on 28 May 2020).

230. Tarasov, V.N. Hydroelastic vibrations of hydropower units of hydro power plant. *Hydraul. Eng.* **2012**, *1*, 26–36. (In Russian)

231. Toga, A.W.; Thompson, P.M. Mapping brain asymmetry. *Nat. Rev. Neurosci.* **2003**, *4*, 37–48. [CrossRef]

232. Sun, T.; Walsh, C.A. Molecular approaches to brain asymmetry and handedness. *Nat. Rev. Neurosci.* **2006**, *7*, 655–662. [CrossRef]

233. Grove, E.A.; Fukuchi-Shimogori, T. Generating the cerebral cortical area map. *Annu. Rev. Neurosci.* **2003**, *26*, 355–380. [CrossRef]

234. Geschwind, D.H.; Miller, B.L. Molecular approaches to cerebral laterality: Development and neurodegeneration. *Am. J. Med. Genet.* **2001**, *101*, 370–381. [CrossRef]

235. Corballis, M.C. Mirror-Image Equivalence and Interhemispheric Mirror-Image Reversal. *Front. Hum. Neurosci.* **2018**, *12*, 140. [CrossRef]

236. Stoyanov, Z.; Decheva, L.; Pashalieva, I.; Nikolova, P. Brain asymmetry, immunity, handedness. *Open Med.* **2012**, *7*, 1–8. [CrossRef]

237. Corballis, M.C. Bilaterally Symmetrical: To Be or Not to Be? *Symmetry* **2020**, *12*, 326. [CrossRef]

238. Corballis, M.C.; Beale, I.L. *The Psychology of left and Right*; Lawrence Erlbaum Associates: Hillsdale, NJ, USA, 1976; p. 240.

239. Needham, R. *Right and Left: Essays on Dual Symbolic Classification*; University of Chicago Press: Chicago, IL, USA, 1973. Available online: https://muse.jhu.edu/article/598336/pdf (accessed on 28 May 2020).

240. Lozano, M.; Estalrrich, A.; Bondioli, L.; Fiore, I.; Bermudez de Castro, J.M.; Arsuaga, J.L.; Carbonell, E.; Rosas, A.; Frayer, D.W. Right-handed fossil humans. *Evol. Anthropol.* **2017**, *26*, 313–324. [CrossRef] [PubMed]

241. Rizzolatti, G.; Craighero, L. The mirror-neuron system. *Annu. Rev. Neurosci.* **2004**, *27*, 169–192. [CrossRef] [PubMed]

242. Casile, A. Joining forces: Motor control meets mirror neurons: Comment on "Grasping synergies: A motor-control approach to the mirror neuron mechanism" by D'Ausilio, Bartoli, and Maffongelli. *Phys. Life. Rev.* **2015**, *12*, 111–113. [CrossRef] [PubMed]

243. Rizzolatti, G.; Sinigaglia, C. The mirror mechanism: A basic principle of brain function. *Nat. Rev. Neurosci.* **2016**, *17*, 757–765. [CrossRef]

244. Iacoboni, M. Imitation, empathy, and mirror neurons. *Annu. Rev. Psychol* **2009**, *60*, 653–670. [CrossRef]

245. Ulmer, S.; Mooser, A.; Blaum, K.; Braeuninger, S.; Franke, K.; Kracke, H.; Leiteritz, C.; Matsuda, Y.; Nagahama, H.; Ospelkaus, C.; et al. The magnetic moments of the proton and the antiproton. *J. Phys. Conf. Ser.* **2014**, *488*, 1–7. [CrossRef]

246. Ulmer, S.; Mooser, A.; Nagahama, H.; Sellner, S.; Smorra, C. Challenging the standard model by high-precision comparisons of the fundamental properties of protons and antiprotons. *Philos. Trans. A Math. Phys. Eng. Sci.* **2018**, *376*, 1–12. [CrossRef]

247. Nagahama, H.; Smorra, C.; Sellner, S.; Harrington, J.; Higuchi, T.; Borchert, M.J.; Tanaka, T.; Besirli, M.; Mooser, A.; Schneider, G.; et al. Sixfold improved single particle measurement of the magnetic moment of the antiproton. *Nat. Commun.* **2017**, *8*, 14084. [CrossRef]

248. Davankov, V. Chirality as an inherent general property of matter. *Chirality* **2006**, *18*, 459–461. [CrossRef]

249. Davankov, V.A. Biological Homochirality on the Earth, or in the Universe? A Selective Review. *Symmetry* **2018**, *10*, 749. [CrossRef]

250. Kozyrev, N.A. *On the Possibility of Experimental Investigation of the Properties of Time*; Time and Philosophy: Prague, Czech Republic, 1971; pp. 111–132.

251. Kozyrev, N.A. *Selected Works*; Leningrad State University: Saint Petersburg, Russia, 1991; p. 488. (In Russian)

252. Kozyrev, N.A. Possibility of experimental study of the properties of time. *Abraham Zelmanov J.* **2012**, *5*, 188–220.

253. Margerison, T. *Causal Mechanics—The Russin Scientific Dispute*; New Scientists: London, UK, 1959.

254. Levich, A.P. *A Substantial Interpretation of N. A. Kozyrev's Conception of Time*; World Scientific: Hackensack, NJ, USA, 1996; pp. 1–42.

255. Kasatkina, E.A.; Shimolov, O.L.; Raspopov, O.M. Ozone "mini-holes" initiated by solar protons in the northern and southern polar caps. *Geomagnetism Aeronomiya* **1998**, *38*, 30–36.

256. Sabburg, J.; Parisi, A.; Wong, J.; Meldrum, L. Preliminary UV, ozone and cloud comparison between Southern and Northern Hemisphere, sub-tropical latitude sites during 1996/1997. *J. Atmos. Solar Terr. Phys.* **2001**, *63*, 1623–1629. [CrossRef]

257. Watt-Meyer, O.; Frierson, D.M.W.; Fu, Q. Hemispheric Asymmetry of Tropical Expansion Under CO_2 Forcing. *Geophys. Res. Lett.* **2019**, *46*, 9231–9240. [CrossRef]

258. Dunn, R.R.; Agosti, D.; Andersen, A.N.; Arnan, X.; Bruhl, C.A.; Cerda, X.; Ellison, A.M.; Fisher, B.L.; Fitzpatrick, M.C.; Gibb, H.; et al. Climatic drivers of hemispheric asymmetry in global patterns of ant species richness. *Ecol. Lett.* **2009**, *12*, 324–333. [CrossRef]